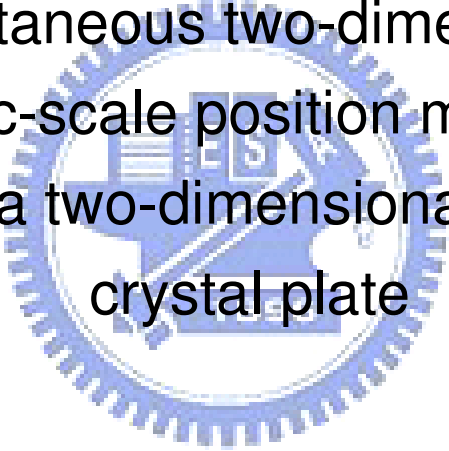


國立交通大學  
光電工程研究所  
碩士學位論文

透過二維光子晶體來監控二維奈米級的  
位置變化

Simultaneous two-dimensional  
nanometric-scale position monitoring by  
probing a two-dimensional photonic  
crystal plate



研究生：鍾佩芳

指導教授：賴暎杰

中華民國九十八年六月

Simultaneous two-dimensional nanometric-scale position  
monitoring by probing a two-dimensional photonic crystal  
plate

研究生：鍾佩芳

Student : Pei-Fang Chung

指導教授：賴暎杰 老師

Advisor : Yin-Chieh Lai



A Thesis

**Submitted to Institute of Electronics College of Engineering  
National Chiao Tung University  
in partial Fulfillment of the Requirements  
for the Degree of  
Master  
In Electro-Optical Engineering**

**June 2009**

**Hsinchu, Taiwan, Republic of China**

中華民國九十八年六月

# 摘要

論文名稱：透過二維光子晶體來監控二維奈米級的位置變化

校所別：國立交通大學光電工程研究所

頁數：1 頁

畢業時間：九十七學年度第二學期

學位：碩士

研究生：鍾佩芳

指導教授：賴暎杰 老師

關鍵詞：位置監控、光子晶體、干涉、光學量測

在本論文中，我們提出一套簡易及低成本的干涉系統，藉著由偵測二維六角型光子晶體玻璃基板來即時監控二維之奈米等級位移量。這個即時監控二維奈米等級位移量的方法，是將波長為 633-nm 的氦氖雷射光源正向入射一個二維六角型光子晶體玻璃基板來產生遠場繞射光束。基板在作二維移動時，六道繞射光束的光場相位會隨著光子晶體玻璃基板的位移向量來作線性變動。當我們取兩道一階繞射光束與零階光束在兩個正交平面上形成二維的干涉圖形，利用 CCD 讀取並作訊號處理來量得移動前後之相位差，即可推算出裝置基板之移動平台的位移量，其量測二維位移量之準確度可到達奈米等級。最小可測量的位置變化量會與作為繞射光柵的光子晶體之週期大小有關，而我們所用的二維光子晶體週期約為  $1.28\mu\text{m}$ ，最小可量測的位置變化量可到 20nm。

# ABSTRACT

Title : Simultaneous two-dimensional nanometric-scale position monitoring  
by probing a two-dimensional photonic crystal plate

Pages : 1 Page

School : National Chiao Tung University

Department : Institute of Electro-Optical Engineering

Time : June, 2009

Degree : Master

Researcher : Pei-Fang Chung

Advisor : Prof. Yin-Chieh Lai

Keywords : position monitor · Photonic crystal · Interferometer · Optical  
measurement



In this thesis, simultaneous two-dimensional nanometric-scale position monitoring is achieved in a simple and cost-effective interferometric setup by real-time probing a two-dimensional hexagonal photonic crystal glass substrate. To real-time monitor the two-dimensional translational movement in nanometric-scale, an optical imaging system is built by probing a hexagonal photonic crystal glass (HPCG) with a 633-nm He-Ne laser beam. The translation movements in both directions are recorded in the phases of the fields of the diffracted six spots in a linear relation. By carefully aligning the two first-order spots and the zero-order spot to form chessboard-like interference pattern on the CCD camera, the individual nanometric-scale movement information can be determined by the phase change of the chessboard-like interference pattern before and after moving. In principle it can attain the

nanometric-scale accuracy of position reading in both orthogonal moving directions. The minimum detectable translational movement is dependent on the period of the probed photonic crystal ( $1.28\mu\text{m}$  in this study) and can be down to 20nm as demonstrated in the present work.



# ACKNOWLEDGEMENT

在交大兩年的碩士生活裡，最要感謝的是賴暎杰老師的細心指導，老師總是不厭其煩地解答我的疑惑，從賴老師身上學到的不只是知識上的收穫，還有在求學與研究時應有的態度。

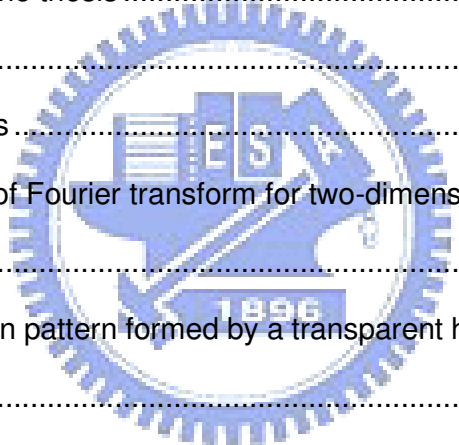
感謝徐桂珠學姊對我全心全力地教導與幫助，尤其學姊傳授的實驗經驗大大地幫助我完成這個實驗。還要感謝陳南光學長、周森益學長、項維巍學長、郭立強學長、許宜蕙學姊、鞠曉山學長、莊佩蓁學姊、張宏傑學長、辛宸瑋學姊以及電子所李逸哲學長，在實驗上給予我的協助，另外，感謝在課業上一起學習、一起分享校園生活點滴的朋友們，昱勳、子翔、秀鳳、柏萱、家豪、柏歲、姿媛，感謝大家讓我的研究生生活充滿歡笑。

最後，感謝在生活上幫我分憂解勞的凱婷、佩蓁，還有總是支持我的家人和朋友們，謝謝大家！

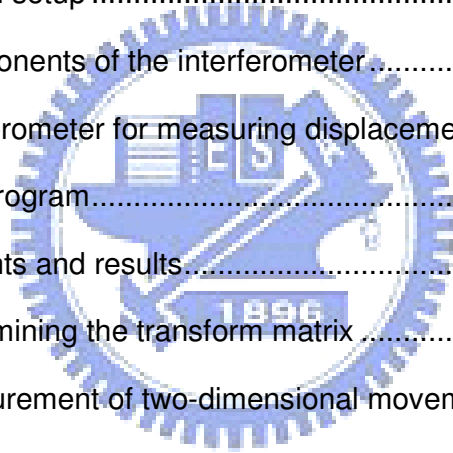


# CONTENTS

ABSTRACT( in Chinese) .....	i
ABSTRACT (in English) .....	ii
ACKNOWLEDGEMENT .....	iv
CONTENTS.....	v
LIST OF FIGURES .....	vii
Chapter 1 : Introduction.....	1
1.1 Review of displacement measuring method .....	1
1.2 Motivation of the thesis .....	2
1.3 Structure of the thesis .....	3
1.4 References .....	4
Chapter 2 : Principles .....	6
2.1 Introduction of Fourier transform for two-dimensional periodic function .....	6
2.2 The diffraction pattern formed by a transparent hexagonal-lattice glass .....	7
2.2-1 Introduction of diffraction .....	7
2.2-2 The diffraction pattern produced by probing a hexagonal photonic crystal glass .....	8
2.2-3 The phase variation of diffraction beams after moving diffraction grating.....	10
2.3 Obtain the displacement from interference pattern .....	11
2.3-1 The relation between phase variation and displacement.....	11
2.3-2 Properties of the spectrum .....	15
2.4 The transform matrix for obtaining displacement from phase variation .....	16



2.5 References .....	16
Chapter 3 : Experiment of one-dimensional measurement .....	18
3.1 Experimental setup .....	18
3.1-1 Fabrication of a transparent hexagonal-lattice glass .....	18
3.1-2 Experimental setup.....	20
3.1-3 Observing variation by rotating diffraction grating .....	21
3.2 Measurement procedures and results.....	22
3.3 References .....	25
Chapter 4 : Experiment of two-dimensional measurement.....	26
4.1 Experimental setup .....	26
4.1-1 Components of the interferometer.....	26
4.1-2 Interferometer for measuring displacement in two-dimension	28
4.2 Monitoring program.....	32
4.3 Measurements and results.....	37
4.3-1 Determining the transform matrix .....	37
4.3-2 Measurement of two-dimensional movement .....	41
4.3-3 Analysis .....	42
4.3-4 Discussion .....	45
4.4 References .....	47
Chapter 5 : Conclusions and future work .....	48
5.1 Conclusions .....	48
5.2 Future work.....	48





# LIST OF FIGURES

Fig.2.1	The picture of experimental setup and the diffraction image.....	9
Fig.2.2	(a) Sketches of a hexagonal-lattice glass and (b) the corresponding first-order diffraction pattern. ....	9
Fig.2.3	The interference pattern (a) before and (b) after moving the diffraction grating.....	12
Fig. 2.4	The schema of spatially varying function and its spectrum (a)The function spatially varying in the x-direction(b) The spectrum of sinusoidal function which varies in the x-direction(c) The function spatially varying in the y-direction(d) The spectrum of sinusoidal function which varies in the y-direction(e) Idealized surface-height variation of field .....	14
Fig.3.2	Schematic diagram of the 1-D displacement measurement.....	21
Fig.3.3	The actual system of the 1-D displacement measurement.....	21
Fig.3.4	Typical 1D interference pattern captured by CCD, the pattern after processing and the calculated phase distribution. ....	23
Fig.3.5	Number of period versus translational distance for HPCG crystal axis placed at 0° and 60°. ....	24
Fig.3.6.	One-dimensional position monitoring statistics according to the amount of phase shifts with respect to one period.....	25
Fig.4.1	Beam expander .....	27
Fig.4.2	Schematic diagram of the experimental setup for two-dimensional measurement.....	29
Fig.4.3	The actual experimental setup for two-dimensional measurement..	29
Fig.4.4	The actual optical diffraction image of diffraction pattern in	

two-dimensional measurement.....	30
Fig. 4.5 The image transformed from the measured chessboard-like interference pattern by the LabVIEW software.....	34
Fig.4.6 The flow chart for FFT algorithm .....	34
Fig.4.7 The complex spatial-frequency spectrum of the interference pattern .....	35
Fig.4.8 The filtered interference pattern (a) in the x-direction (b) in the y-direction. ....	36
Fig.4.9 The original plot of phase-changes versus displacement(a) Variation of x displacement with x phase change(b) Variation of x displacement with y phase change(c) Variation of y displacement with x phase change(d) Variation of y displacement with y phase change.....	38
Fig.4.10 The chart of phase-changes versus displacement after correcting the phase-change value(a) Variation of x displacement with x phase change(b) Variation of x displacement with y phase change(c) Variation of y displacement with x phase change(d) Variation of y displacement with y phase change .....	40
Fig.4.11 The results of two-dimensional measurements by probing the HPCG plate. Red one presents stage displacements, and black one presents measured displacements.....	41
Fig.4.12 Statistics for sets of two-dimensional movements .....	42
Fig.4.13 Comparison between two different methods (a) scanning the HPCG plate randomly, (b) scanning it into certain small area. ....	43
Fig. 4.14 To make the BCSG on a PET film, a mechanically grooved structure was first formed on a printing roller using a roller cutter with the designed profile as shown in (a).Then the UV resin was dispensed on	

the PET film, imprinted by the roll, and cured with UV source as shown in (b). ..... 44

Fig.4.15 The diffraction pattern of probing the blazed grating ..... 45

Fig.4.16 The statistics of measurement by probing a blazed diffraction grating, the period of which is  $85\mu\text{m}$ ..... 45

Fig.4.17 The disturbance of phase caused by environment (a) in the x-direction (b) in the y-direction ..... 46



# Chapter 1

## Introduction

### 1.1 Review of displacement measuring method

Optical measurement techniques have received increased attention in the past years because in general optical methods have many advantages over other measuring methods. They are usually non-invasive, capable of observing highly transient phenomena and can have high spatial and temporal resolution. Precision measurement of displacement or position has played an important role in semiconductor technology, nanotechnology, biotechnology, and so on. It is expected that optical precision measurement techniques for displacement or other physical quantities will continue to be important in many new fields of technologies.

In the past several optical interferometer techniques have been widely used for precision measurement of displacement. They include the heterodyne interferometers [1-1]-[1-2], homodyne interferometers [1-3]-[1-4], grating interferometers [1-5]-[1-7], and heterodyne grating interferometers [1-8]. Among them, a high resolution of 0.2 nm has been achieved by a heterodyne grating interferometer system. Besides interferometers, there are some other methods without analyzing the interference fringe shift. For example, they can be by monitoring the changes in the intensity of the light reflected from a variable-air-gap optical waveguide [1-9], or be an astigmatic detection system with a modified digital-versatile-disk optical head [1-10].

Generally, in a displacement measurement system with a grating, a coherent light beam is emitted into the grating so that a plurality of diffraction beams are generated. Parts of the diffraction beams interfere with a reference light beam, so that periodic interference fringes are formed. Accordingly, when the grating moves, the displacement of the grating is calculated from the variation of the above-described

interference fringes. However, when the related technology was initially developed, the above-described displacement measurement system is simply used to measure the displacement in one-dimension due to the fabricating technique of the grating.

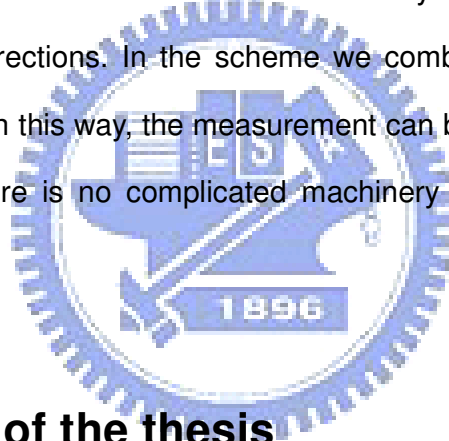
With the development of related technologies, multi-dimensional displacement measurement systems can also be provided. For example, in a displacement measurement system, gratings at a predetermined period respectively serve as alignment marks for the corresponding displacement in each dimension, so that the actual displacements are measured and recorded. Further, in a displacement measurement system, the actual displacements in each dimension are obtained by detecting the amplitude changes of the interference fringes in each dimension. In the above-described multi-dimensional displacement measurement system, a plurality of photo sensors disposed in each dimension are used to read the amplitudes of the interference fringes for obtaining the actual displacements in each dimension, which in practice gives rise to an increase in costs and complexity of the whole displacement measurement system. Furthermore, the displacement measurement system having many photo sensors may be difficult to be applied in practice.

## 1.2 Motivation of the thesis

The recent rapid progress of nanophotonics researches urgently requires the technique to control the position of objects with nanometric precision. There is an increasing demand for measuring long-range displacement with nanometric resolution. The nanometric-scale position monitoring method in the literature mainly combines the delicate optical methods with mechanical tuning elements. Though the best achievable resolution can reach nanoscale, the above methods suffer from not only the limitation of detection length but also the lack of simultaneous two- or even

three-dimensional displacement measurement in a simple setup. Besides, traditional measurement system for two-dimensional movement is composed of two sets of one-dimensional measurement system, which means that two sets of analyzing devices are applied. For example, a planar encoder is proposed for sensing the two-dimensional displacement of a two-dimensional grating [1-5]. In this system, two phase-shift detection modules are provided to respectively analyze the x-and y-measurement.

In our work, a simple way to achieve simultaneous two-dimensional nanometric-scale position monitoring is proposed and demonstrated, which in principle can attain the nanometric-scale accuracy of position reading in both orthogonal moving directions. In the scheme we combine three beams to yield an interference pattern. In this way, the measurement can be achieved by only one CCD camera. Besides, there is no complicated machinery or expensive devices in our system [1-11]-[1-13].



### **1.3 Structure of the thesis**

The present thesis comprises five chapters. Chapter 1 is an introductory chapter consisted of an introduction to optical precision measurements and the motivation of our research. Chapter 2 describes the principles and analysis of our research work. We explain how the optical phase variation results from the grating displacement. It contains the theory of Fourier transform method, analysis of phase variation, and the behavior of interference patterns. Chapter 3 describes our experimental procedures for one-dimensional displacements, and shows the measurement results. Chapter 4 describes the procedures for two-dimensional position monitoring, and discusses the measurement results. Finally, chapter 5 gives the conclusions and discusses possible

future works.

## 1.4 References

- [1-1] F.C. Demarest, “High-resolution, high-speed, low data age uncertainty, heterodyne displacement measuring interferometer electronics” , Meas. Sci. Technol. 9, 1024–1030 (1998).
- [1-2] C.W. Wu, “Heterodyne interferometric system with subnanometer accuracy for measurement of straightness” , Appl. Opt. 43, 3812–3816 (2004).
- [1-3] L. Salbut, “Waveguide grating (moiré) microinterferometer for inplane displacement/strain field investigation”, Opt. Eng. 41, 626 (2002)
- [1-4] X. Liu, W. Clegg, D.F.L. Jenkins, B. Liu, “Polarization interferometer for measuring small displacement” , IEEE Trans. Instrum. Meas. 50, 868–871 (2001).
- [1-5] C.-F. Kao, C.-C. Chang, M.-H. Lu, “Double-diffraction planar encoder by conjugate optics”, Opt. Eng. 44, 023063 (2005).
- [1-6] H. Huan, O. Sasaki, T. Suzuki, “Movement measurement with a grating interferometer using sinusoidal phase-modulation”, Opt. Commun. 267, 341-346 (2006).
- [1-7] C.-C. Hsu, C.-C. Wu, J.-Y. Lee, H.-Y. Chen, H.-F. Weng, “Reflection type heterodyne grating interferometry for in-plane displacement measurement”, Opt. Commun. 281, 2582-2589 (2008)
- [1-8] J.-Y. Lee, H.-Y. Chen, C.-C. Hsu, C.-C. Wu, “Optical heterodyne grating interferometry for displacement measurement with subnanometric resolution”, Sens.Actuators A 137, 185-191 (2007).
- [1-9] E.-T. Hwu, et al., “Simultaneous detection of translational and angular displacements of micromachined elements”, App. Phys. Lett. 91, 221908(2007).

[1-10] F. Chen, et al., "Nanoscale displacement measurement in a variable-air-gap optical waveguide", App. Phys. Lett. 88, 161111(2006).

[1-11] B. V. Grop, A.G. Onaran, F. L. Degertekin, "Integrated dual grating method for extended range interferometric displacement detection in probe microscopy", App. Phys. Lett. 91, 083101 (2007).

[1-12] W. Lee, N. A. Hall, F. L. Degertekin, "A grating-assisted resonant-cavity-enhanced optical displacement detection method for micromachined sensors", App. Phys. Lett. 85, 3032 (2004).

[1-13] T. Yu, H. Li, Z. Cao, Y. Wang, Q. Shen, Y. He, "Oscillating wave displacement sensor using the enhanced Goos-Hanchen effect in a symmetrical metal-cladding optical waveguide", Opt. Lett. 33, 1001 (2008).





# Chapter 2

## Principles

The aim of this thesis is to real-time monitor the two-dimensional translational movement in nanometric-scale. Thus an optical imaging system is built by probing a hexagonal photonic crystal glass (HPCG). The translation movements in both directions are recorded in the phases of the fields of the diffracted spots. By carefully aligning the first-order two spots and the zero-order spot to form chessboard-like interference pattern, the individual nanometric-scale movement information can be determined by the phase change of the chessboard-like interference pattern before and after moving.

In this Chapter, the principles of how to determine the individual nanometric-scale movement information are described. The first part is a brief introduction of Fourier transform for two-dimensional periodic functions. It is then followed by the mathematical model to express the diffraction pattern formed by a transparent hexagonal-lattice glass. The third part is to explain how to obtain the displacement from interference pattern, and the final part is to introduce the transform matrix for obtaining displacement from phase variation.

### 2.1 Introduction of Fourier transform for two-dimensional periodic function

If a two-dimensional function  $f(x, y)$  satisfies the Dirichlet conditions, it can be decomposed into a linear combination of complex exponentials according to

$$f(x, y) = \int_{-\infty}^{\infty} \int_{-\infty}^{\infty} F(\zeta, \eta) e^{j2\pi(\zeta x + \eta y)} d\zeta d\eta \quad (2.1)$$

Here  $F(\zeta, \eta)$  is given by

$$F(\zeta, \eta) = \int_{-\infty}^{\infty} \int_{-\infty}^{\infty} f(\alpha, \beta) e^{-j2\pi(\alpha\zeta + \beta\eta)} d\alpha d\beta \quad (2.2)$$

and is known as the two-dimensional Fourier transform of  $f(x, y)$ , with  $\zeta$  and  $\eta$  being the spatial-frequency variables corresponding to the  $x$ - and  $y$ -directions, respectively. This function is also called the complex spatial-frequency spectrum of  $f(x, y)$ , or more simply, its spectrum. It is the spatial frequency domain representation of  $f(x, y)$ .

The number of oscillations made by a time-varying sine wave per unit time is described as the temporal frequency of the function. For a function that varies sinusoidally with some spatial coordinate, the spatial frequency associated with the function in that same direction indicates the number of repetitions the function makes per unit distance [2-1]

## 2.2 The diffraction pattern formed by a transparent hexagonal-lattice glass

### 2.2-1 Introduction of diffraction

There are two types of diffraction phenomena, known as Fraunhofer diffraction (or far-field diffraction, appears far from the aperture) and Fresnel diffraction (or near-field diffraction, appears close to the aperture). The Fraunhofer diffraction occurs when the source of light and the screen are effectively at infinite distances from the aperture or obstacle that causes diffraction. Mathematically, Fraunhofer diffraction occurs when :

$$F = \frac{a^2}{L\lambda} \ll 1 \quad (2.3)$$

where  $a$  is slit size,  $\lambda$  is wavelength and  $L$  is distance from the aperture.

In this experiment, the period of the hexagonal photonic crystal glass (HPCG) plate is

1.28 $\mu$ m and the wavelength of the source laser beam is 633nm. Since the outgoing waves of the HPCG plate are planar on the image plane, it is a Fraunhofer diffraction scheme.

## **2.2-2 The diffraction pattern produced by probing a hexagonal photonic crystal glass**

A repetitive array of diffracting elements, either apertures or obstacles, that has the effects of producing periodic alterations in the phase, amplitude, or both of the emergent wave is said to be a diffraction grating. In our measurement, the hexagonal photonic crystal glass is regarded as a diffraction grating [2-3].

The organization of the hexagonal photonic crystal glass is qualitatively characterized by focusing the He-Ne laser beam on the sample. Fig.2.1 displays the experimental setup for observing the diffraction pattern. The laser beam was focus onto a transparent hexagonal photonic crystal glass plate for normal incidence. The imaging system of the prepared sample is located at the focal point of a converging lens with 125-mm-long focal length. In the diffraction image shown on Fig.2.1, the center spot is the zero-order diffraction beam, and the surrounding six spots are the first-order diffraction beams. The first-order diffraction angle can be figured out from the following expression :

$$a \sin \theta_m = m\lambda, \quad m=0, \pm 1, \pm 2, \dots \quad (2.4)$$

Where  $a$  is the period of a HPCG plate,  $\lambda$  is the wavelength of the laser beam, and  $m$  is the order of diffraction beam. It is known as the grating equation for normal incidence. According to Eq.2.4, the first-order diffraction angle  $\theta$  can be calculated to be 27.96°. Also, it can be found experimentally that  $\theta=26.56^\circ$  from the way of geometry analysis.

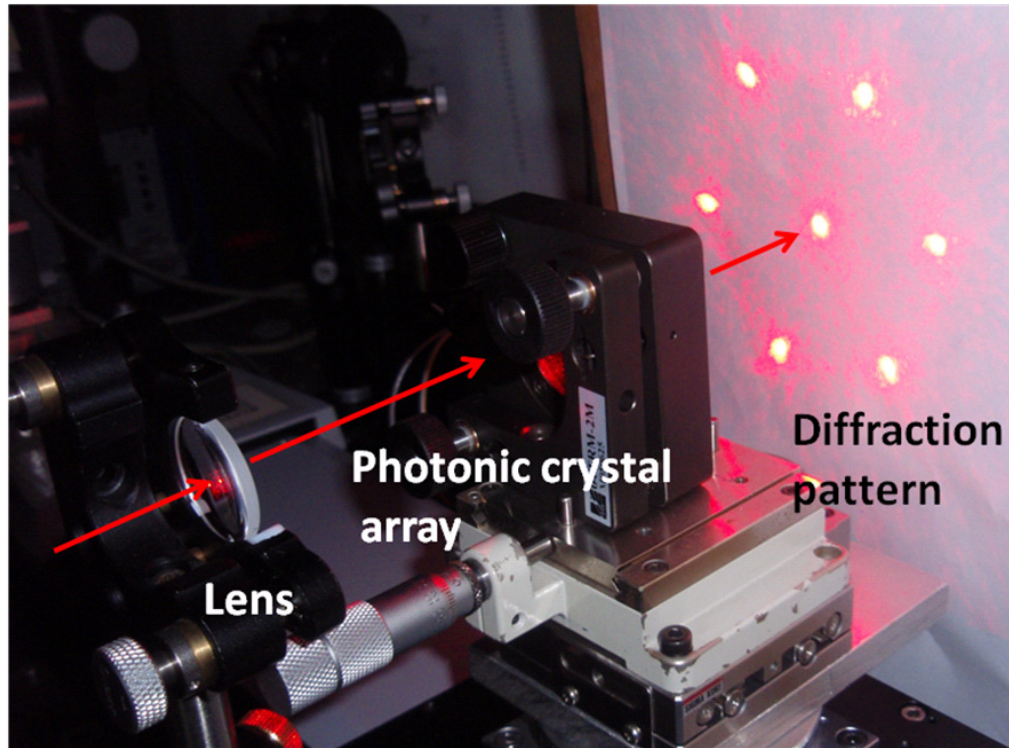


Fig.2.1 The picture of experimental setup and the diffraction image.

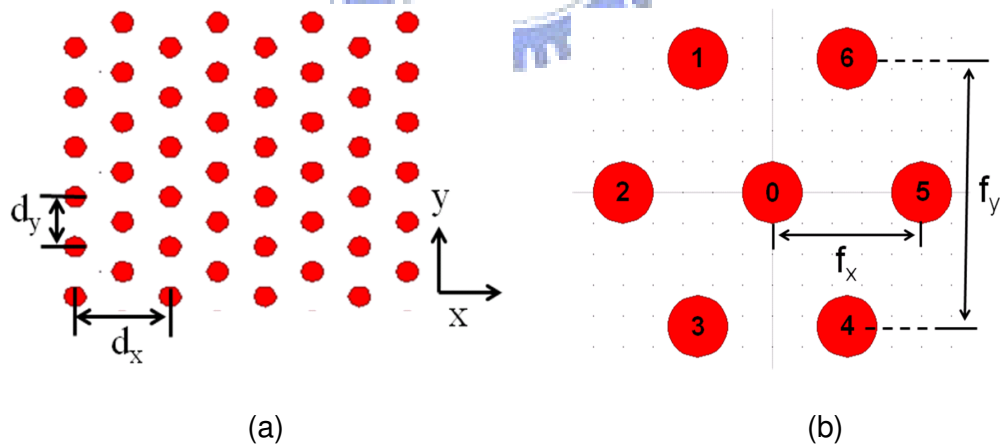


Fig.2.2 (a) Sketches of a hexagonal-lattice glass and (b) the corresponding first-order diffraction pattern.

Fig. 2.2 shows the sketches of the structure of a hexagonal-lattice glass and the diffraction pattern. According to Fig.2.2 (a), the transmittance of the HPCG plate can

be written in general as follows :

$$t(x, y) = g(x, y) \otimes \left[ \text{comb}\left(\frac{x}{d_x}\right) \text{comb}\left(\frac{y}{d_y}\right) + \text{comb}\left(\frac{x}{d_x} - \frac{1}{2}\right) \text{comb}\left(\frac{y}{d_y} - \frac{1}{2}\right) \right] \quad (2.5)$$

Here  $t(x, y)$  denotes transmittance of the photonic crystal array,  $d_x$  and  $d_y$  are the periods of the array along the x- and y- directions as shown on Fig.2.2(a), and  $g(x, y)$  is the transmittance on one unit cell.

The Fraunhofer far field diffraction pattern of such a plate under normal plane wave incidence is simply the Fourier transform of the distribution across the aperture (i.e., the transmittance function). Therefore, we process the transmittance function by Fourier transform to obtain the scaled far field distribution. The Fourier transform of the transmittance function can be expressed in the following form :

$$u_f(f_x, f_y) = F\{t(x, y)\}$$

$$u_f(f_x, f_y) = \sum_{m,n} G\left(f_x - \frac{n}{d_x}, f_y - \frac{m}{d_y}\right) (1 + e^{i\pi(m+n)}) \quad (2.6)$$

Here  $f_x$  and  $f_y$  are the spatial frequencies of the image along the x- and y- directions as shown on Fig.2.2 (b) and  $G$  is the Fourier transform of  $g(x, y)$ . It is interesting to note that the interference term in the right hand side gives rise to the hexagonal distribution in the Fourier domain for a hexagonal structure.

### 2.2-3 The phase variation of diffraction beams after moving diffraction grating

The relation between phase variations and displacements can be directly understood from the translation property of Fourier transform, which states that a translation of the input function  $g(x)$  changes the phase of the transformed function as follows :

$$F\{g(x + x_0)\} = G(f)e^{i2\pi fx_0} \quad (2.7)$$

It shows that the movement information is encoded in the phase term of the Fourier components in a linear relation.

In two-dimension, when the translation in position is applied, similarly, the phases of the far field components carry the position movement information. According to Eq.2.7, if the two-dimensional translation  $x_1$  and  $y_1$  are simultaneously applied, the new diffraction field can be expressed in the following form :

$$\begin{aligned} u_f'(f_x, f_y) &= u_f(f_x, f_y)e^{i2\pi f_x x_1} e^{i2\pi f_y y_1} \\ &= u_{0f}(f_x, f_y)e^{i\delta_0} + u_{1f}(f_x, f_y)e^{i\delta_1} + u_{2f}(f_x, f_y)e^{i\delta_2} + \dots \end{aligned} \quad (2.8)$$

Where  $u_{0f}(f_x, f_y), u_{1f}(f_x, f_y), u_{2f}(f_x, f_y)$  are the original scaled far field distribution of spot 0, spot 1, spot 2 donated in Fig.2.2 (b) and  $\delta_0, \delta_1$  and  $\delta_2$  are the phase shifts of spot 0, spot 1 and spot 2 before and after the translation movement. Though the diffracted spots remain the same configuration, the movement information is recorded in the phase terms of the fields. By separately taking the diffracted spot 1 and spot 2 to interfere with the zero-order spot 0, the recorded phase information  $\delta_1$  and  $\delta_2$  can be estimated from the Fourier transform of the 2D interference pattern function.

## 2.3 Obtain the displacement from interference pattern

### 2.3-1 The relation between phase variation and displacement

First, we discuss the condition in one-dimension. When the diffraction grating is moved a small distance  $\Delta y$ , the interference pattern movement is followed as shown in

Fig.2.3. Comparing the pattern before and after the grating moving, the phase change can be calculated. The formula for displacement  $\Delta y$  and phase change  $\Delta \theta$  is expressed as :

$$\Delta \theta = \frac{2\pi n}{d} \Delta y \quad (2.9)$$

where  $d$  is the period of the grating and  $n$  is the order of diffraction. [2-2]

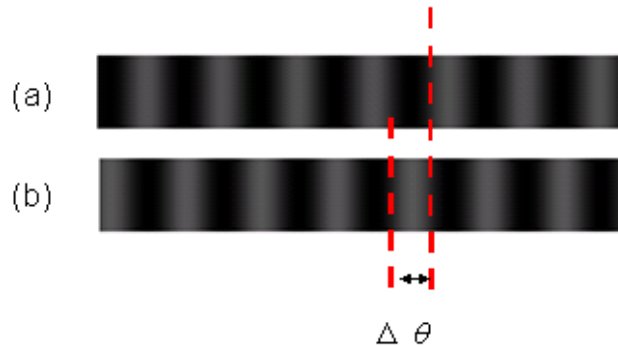


Fig.2.3 The interference pattern (a) before and (b) after moving the diffraction grating

Then, in two-dimension, from Eq.2.8, after moving the diffraction grating, it induces a phase variation in diffraction beams and the interference pattern produced by these diffraction beams will shift. Consider a spatially varying function presenting the interference pattern shown in Fig.2.4 (a) and (c). We assume that the function has a constant background with sinusoidal variation. If we now designate the function to be  $h(x,y)$  and provides a phase shift  $\delta_1$  and  $\delta_2$  respectively in the  $x$ - and  $y$ -directions, we may write

$$h(x, y) = (A + B \cos[2\pi\xi_0(x + \delta_1)])(C + D \cos[2\pi\eta_0(y + \delta_2)]) \quad (2.10)$$

where  $\xi_0$  and  $\eta_0$  are the spatial frequencies in the  $x$ - and  $y$ - directions. The profile of  $h(x, y)$  in  $x$ -direction is shown in Fig.2.4 (e). Notice that  $h(x, y)$  can be put in the form

$$h(x, y) = f(x)g(y) \quad (2.11)$$

where

$$f(x) = A + B \cos[2\pi\zeta_0(x + \delta_1)] \quad (2.12)$$

$$g(y) = C + D \cos[2\pi\eta_0(y + \delta_2)] \quad (2.13)$$

And we see that it is separable in x and y. The spatial-frequency spectrum of h(x, y) is given by

$$\begin{aligned} H(\zeta, \eta) &= \int_{-\infty}^{\infty} \int_{-\infty}^{\infty} h(\alpha, \beta) e^{-j2\pi(\zeta\alpha + \eta\beta)} d\alpha d\beta \\ &= \int_{-\infty}^{\infty} f(\alpha) e^{-j2\pi\zeta\alpha} d\alpha \int_{-\infty}^{\infty} g(\beta) e^{-j2\pi\eta\beta} d\beta \\ &= F(\zeta)G(\eta) \end{aligned} \quad (2.14)$$

Here F(ξ) and G(η) are one-dimensional transform of f(x) and g(y), respectively, and it is apparent that the transform of separable function is itself separable. Thus, with

$$F(\zeta) = [A\delta(\zeta) + \frac{B}{2\zeta_0} \delta\delta(\frac{\zeta}{\zeta_0})] e^{j2\pi\zeta\delta_1} \quad (2.15)$$

$$G(\eta) = [C\delta(\eta) + \frac{D}{2\eta_0} \delta\delta(\frac{\eta}{\eta_0})] e^{j2\pi\eta\delta_2} \quad (2.16)$$

We obtain

$$\begin{aligned} H(\zeta, \eta) &= A\delta(\zeta, \eta) e^{j2\pi\zeta\delta_1} + \frac{B}{2} [\delta(\zeta - \zeta_0, \eta) + \delta(\zeta + \zeta_0, \eta)] e^{j2\pi\zeta\delta_1} \\ &+ C\delta(\zeta, \eta) e^{j2\pi\eta\delta_2} + \frac{D}{2} [\delta(\zeta, \eta - \eta_0) + \delta(\zeta, \eta + \eta_0)] e^{j2\pi\eta\delta_2} \end{aligned} \quad (2.17)$$

And we see that the two-dimensional spectrum of h(x, y) consists of a delta function at the origin, which indicates the constant background, and two others located at  $\xi = \pm\xi_0$  and  $\eta = 0$ , as shown in Fig.2.4(b). The latter two indicate that the function varies sinusoidally in the x-direction, with a frequency of  $\xi_0$ . Similarly, two delta functions are located at  $\xi = 0$  and  $\eta = \pm\eta_0$  as shown in Fig.2.4 (d). This result is an idealization



because of our assumptions on the profile of the function and the fact that we have neglected the finite size of the field [2-1].

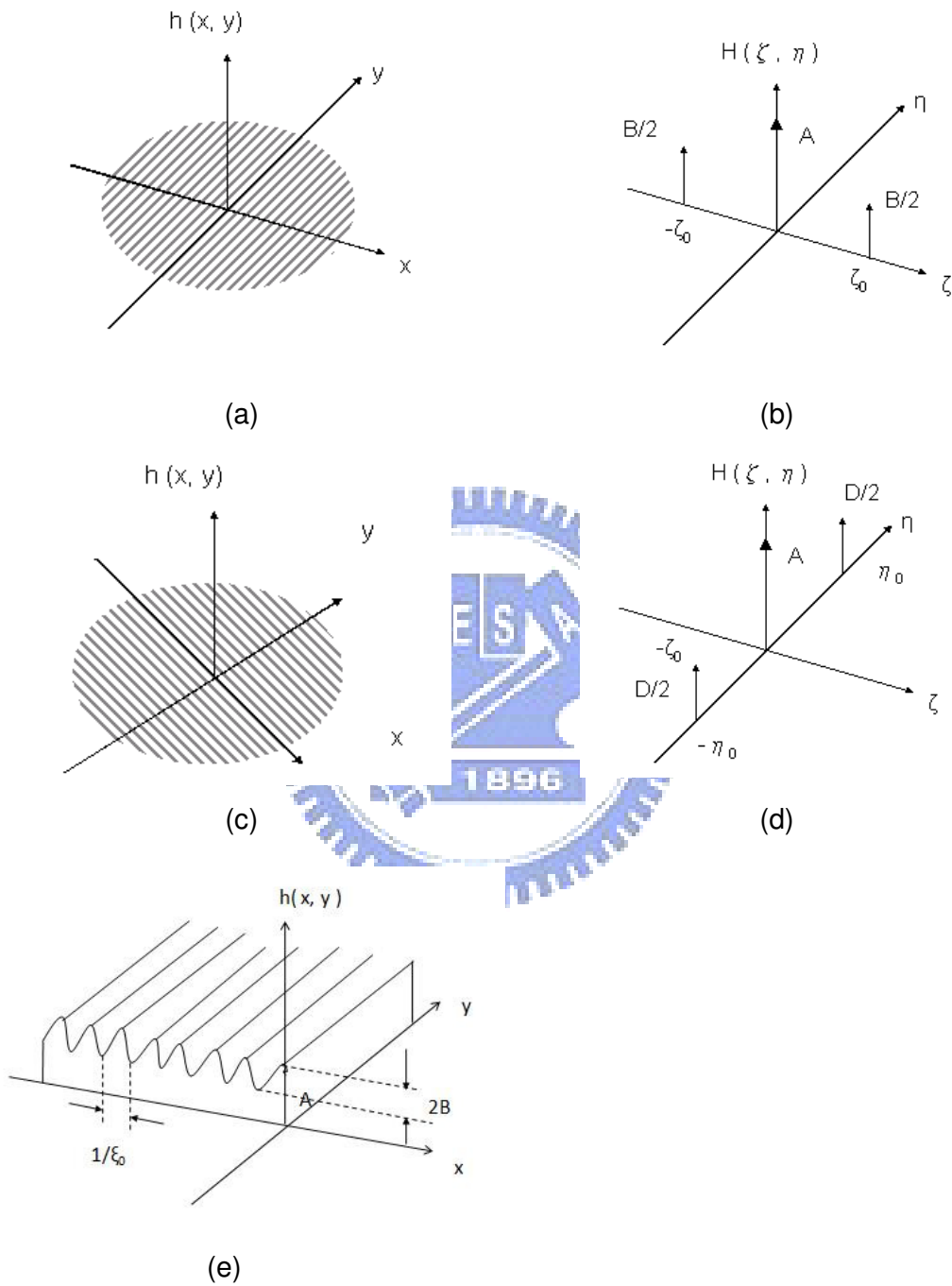


Fig. 2.4 The schema of spatially varying function and its spectrum (a)The function spatially varying in the x-direction(b) The spectrum of sinusoidal function which varies in the x-direction(c) The function spatially varying in the y-direction(d) The

spectrum of sinusoidal function which varies in the y-direction(e) Idealized surface-height variation of field

The movement of the diffraction grating will cause the phase variation of diffraction beams and then the interference pattern produced by these diffraction beams will shift. From Eq.2.17, the shift in the interference pattern can be measured from the spectrum of the interference pattern.

### 2.3-2 Properties of the spectrum

The spectrum resulted from processing a sinusoidal function by Fourier transform is presented above. Here, we introduce some properties of the spectrum.

In Fig.2.4 (a), if the period of the sinusoidal function is increased, the separation  $\xi_0$  decreases. Considering a perfectly sinusoidal function without any constant term added, it has a single frequency component. In other words, the spectrum is a pair of Dirac delta functions located symmetrically with respect to the origin.

The phase  $\phi$  of a real cosinusoidal function  $\cos(\omega_s x + \phi)$  is equal to the complex phase of its spectral component  $\exp[I(\omega_s x + \phi)]$ , which in turn is equal to the complex phase of Fourier transform  $[\delta(\omega - \omega_s) \exp(i\phi)]$  of the cosine function at the frequency  $\omega = \omega_s$ . An important and useful conclusion is that the phase of the real Fourier components of a real function is equal to the complex phase of Fourier transform at the frequency of that component [2-2].

Therefore, the phases  $\delta_1$  and  $\delta_2$  can be identified by taking the arg of the processed data from the complex Fourier component of the interference pattern. In this way, the phase changes of the interference pattern can be inferred from monitoring the phase difference  $\delta_1$  and  $\delta_2$ . Once the phase  $\delta_1$  and  $\delta_2$  are determined, the movement  $x_1$  and  $y_1$  can be decided.

## 2.4 The transform matrix for obtaining displacement from phase variation

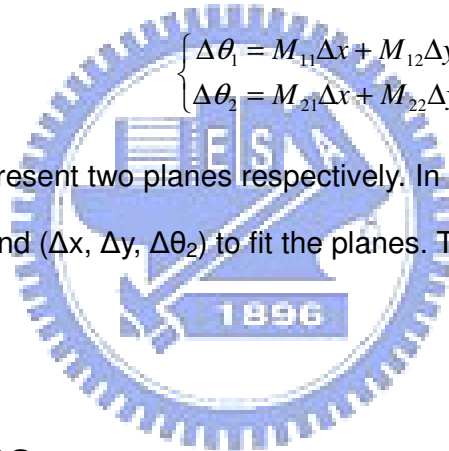
According to Eq.2.9, the relation between movements and phase changes is linear. Therefore, through a two-by-two transform matrix as follows :

$$\begin{bmatrix} \Delta\theta_1 \\ \Delta\theta_2 \end{bmatrix} = \begin{bmatrix} M_{11} & M_{12} \\ M_{21} & M_{22} \end{bmatrix} \begin{bmatrix} \Delta x \\ \Delta y \end{bmatrix} \quad (2.18)$$

The movements in the x- and y- directions can be determined from the two phase variations. The transform matrix also can be expressed in another way shown in the following form :

$$\begin{cases} \Delta\theta_1 = M_{11}\Delta x + M_{12}\Delta y \\ \Delta\theta_2 = M_{21}\Delta x + M_{22}\Delta y \end{cases} \quad (2.19)$$

The two functions represent two planes respectively. In our work, we measure several sets of  $(\Delta x, \Delta y, \Delta\theta_1)$  and  $(\Delta x, \Delta y, \Delta\theta_2)$  to fit the planes. Then, the transform matrix can be found.



## 2.5 References

- [2-1] J. D.Gaskill , "Linear Systems, Fourier Transforms, and Optics", New York Wiley press 1987.
- [2-2] D. Malacara, M. Servin, Z. Malacara, "Interferogram analysis for optical testing", New York Marcel Dekker press 1998.
- [2-3] E. Hecht, "Optics", San Francisco Addison Wesley press 2002.
- [2-4] K.-C. Hsu, C.-C. Chen, C.-H. Chan, P.-F. Chung, Y.-C. Lai, "Simultaneous two-dimensional nanometric-scale position monitoring by probing a two-dimensional photonic crystal plate", OPT 2008, Taipei, paper Sat-S8-03.
- [2-5] G. F. Lothian, "Optics and its uses ", New York Van Nostrand Reinhold

press 1975.

[2-6] D. Malacara (Ed.), " Optical shop testing", New York press 1991

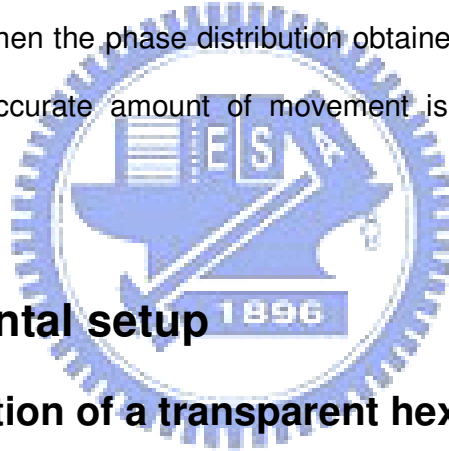
[2-7] R. S. Sirohi, " Optical methods of measurement : wholefield techniques", New York Marcel Dekker press 1999.



# Chapter 3

## Experiment of one-dimensional measurement

To test the nanometric-scale movement detection, the one dimensional position reading is executed first and the experimental results are presented in this Chapter. The sample is mounted on a translation stage comprised of a linear motor stage and a piezoelectric translator (PZT) stage with sub-nm position resolution. The accurate movement of one period is achieved by shifting the translation stage to an approximate distance and then iteratively fine-tuning the PZT stage to match the phase distribution of the interference pattern on the CCD camera. The iteration process terminates when the phase distribution obtained in this step matches that of last step, and the accurate amount of movement is recorded by the Michelson interferometer.

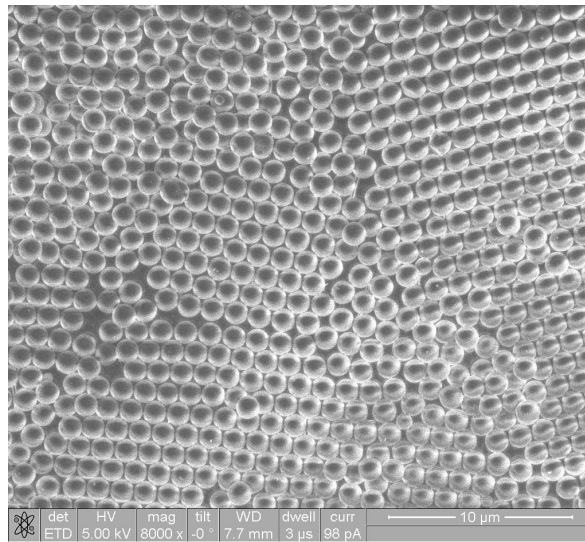


### 3.1 Experimental setup

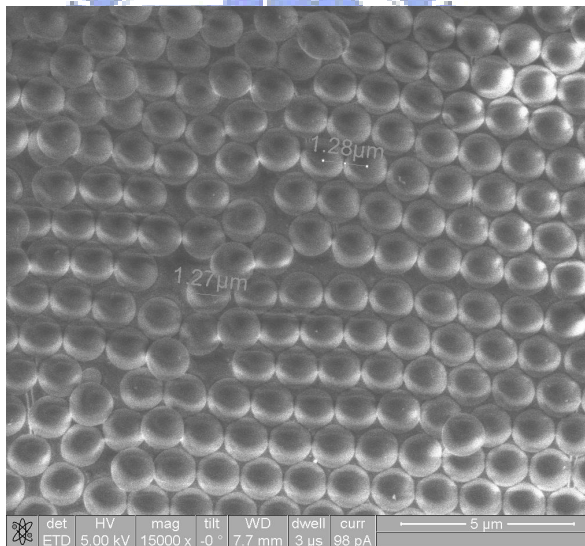
#### 3.1-1 Fabrication of a transparent hexagonal-lattice glass

The hexagonal photonic crystal glass plates used in our experiment are provided by the research group at NCU. They used a closed packing monodisperse polystyrene sphere as a mask, and by different dry etching recipes, the patterns can be transferred into the substrate surface. After etching, a transparent hexagonal photonic crystal glass (HPCG) sample substrate with a large patterned surface was obtained. The sample can be highly uniform over inch square. Since no photolithography process and no vacuum chamber are required, this method is inexpensive and rapid. The period (lattice constant) of the HPCG is determined by the diameter of microspheres, which ranges from 200 nm-700 nm to 1-2 micrometer. The

SEM picture of the surface of a HPCG plate is shown on Fig.3.1. The period is approximately  $1.28\mu\text{m}$ .



(a)



(b)

Fig.3.1 The SEM picture of the surface of a HPCG plate. (a) Overview (b) The period of HPCG is approximately  $1.28\mu\text{m}$ .

In our experiment, the transparent hexagonal-lattice glass is seen as a two-dimensional diffraction grating for measurements. Since the detectable displacement resolution is mainly determined by the grating period, the smaller the

grating period, the higher the resolution of the detectable displacement resolution. Besides, the smaller period of the diffraction grating will produce a bigger diffraction angle, advantageous for us to capture the diffraction beams in shorter distance. As a result of that, the experimental setup can be reduced and simplified.

### **3.1-2 Experimental setup**

The one dimensional position measurement is executed first. The real-time interferometric position monitoring method is based on our previous work in a 1D grating case [3-1]-[3-5]. The whole position monitoring system of one-dimension is illustrated in Fig.3.2. Fig.3.3 shows the actual picture. A single-polarization 633-nm He-Ne laser beam is focused onto the photonic crystal plate with a spherical lens of 125-mm focal length. A 440×480 monochrome CCD camera with a pixel width of 7.15- $\mu\text{m}$  is utilized to record the interference pattern produced by spot 0 (the zero-order beam) and spot 1 (the first-order beam). The sample, a HPCG plate, is mounted on a translation stage comprised of a linear motor stage and a piezoelectric translator (PZT) stage with sub-nm position resolution. By PZT, the sample can be controlled to make one-dimensional movement in the vertical direction of incident beam. And, the accurate amount of movement is recorded by the Michelson interferometer.

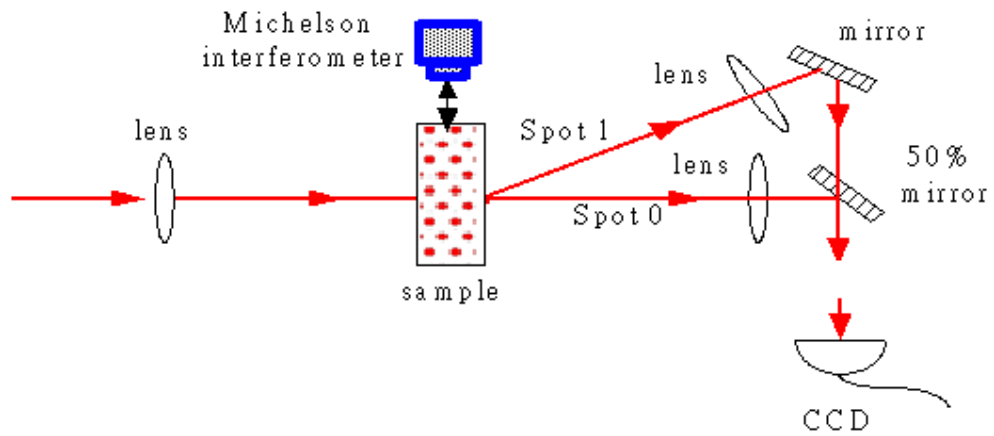


Fig.3.2 Schematic diagram of the 1-D displacement measurement

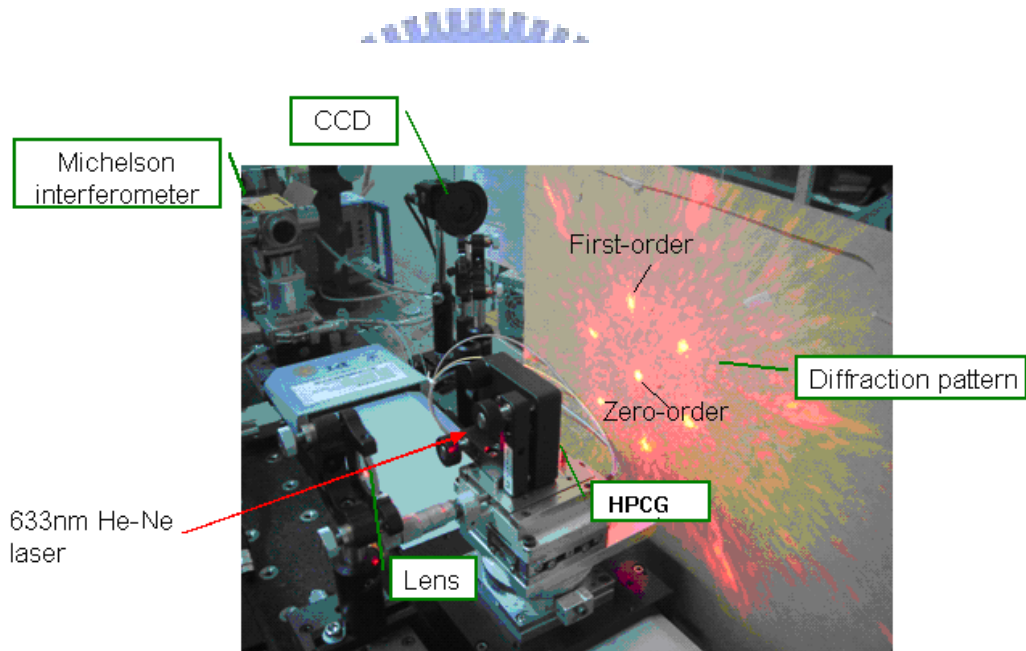


Fig.3.3 The actual system of the 1-D displacement measurement

### 3.1-3 Observing variation by rotating diffraction grating

When rotating the HPCG plate, in principle, the rotation of the six-spot diffracted



image follows. However, the phenomena do not happen in every position of HPCG plate. The diffraction pattern of HPCG plate is not stably produced every time. When the HPCG plate rotates with an increasing angle, approximately to 10 degree, the diffracted image becomes a twelve-spot or other kind of symmetrical pattern. It indicates that the structure of the sample is periodic, but the angle of the axis of the photonic crystal for each area might be different. Therefore, it produces different diffraction patterns and these patterns appear simultaneously. As shown in Fig.3.1 (a), we can find that the arrangement of photonic crystal is periodic in micro square and there are some defects. From another point of view, our system may also provide an optical method for measuring the uniformity of the periodic-patterning samples. Besides, the six-spot diffraction image can exist only when the HPCG plate is in the focal plane of Lens 1.

### 3.2 Measurement procedures and results

One axial slice of the intensity distribution of the interference fringe is recorded on the CCD camera to illustrate the imaging processing algorithm. The visibility of the interference pattern can be optimized by adjusting the polarizer and half-wave plate located on the path of the zero-order beam. The intensity of the first-order diffracted probe beam A is denoted as  $I_A$ , and the intensity of the zero-order beam B is assumed to be  $I_B$ . The intensity distribution of the interference fringe on the CCD along the x-axis, which is perpendicular to the bisector of the two interfering beams, is given by

$$I_{\text{int}} = I_A + I_B + 2\sqrt{I_A I_B} \cdot \cos[kx \cdot 2 \sin(\frac{\theta_2}{2}) + \delta] \quad (3.1)$$

Where  $k=2\pi/\lambda$  is the wave vector,  $\theta_2$  is the interfering angle and  $\delta$  is the phase difference between the two interfering beams. The phase difference  $\delta$  contains two

contributions:

$$\delta = \delta_{\text{caused by grating movement}} + \delta_{\text{path difference}} \quad (3.2)$$

where  $\delta_{\text{caused by grating movement}}$  is the phase change of the diffracted probe beam A caused by the movement of the sample, and  $\delta_{\text{path difference}}$  is the phase change caused by the optical path difference between the zero-order and the first-order beams. Since  $\delta_{\text{path difference}}$  is constant during the scan, the grating phase change (caused by the displacement of the grating) can be inferred from monitoring the phase difference  $\delta$ . The interference pattern  $I_{\text{int}}$  is processed by the Fourier transform to obtain the corresponding spatial frequency spectrum. The spectrum is then filtered to keep only the positive frequency part and is inverse-Fourier-transformed back to the original domain. The phase  $\delta$  can then be identified by taking the arg of the processed data. Figure 3.4 shows the typically resulted periodic pattern along the x-axis captured by the CCD camera (grey solid line), the pattern after the filtering-taking-real-part procedure (grey dotted line) and the obtained phase distribution by taking the arg of the filtered data (bold solid line).

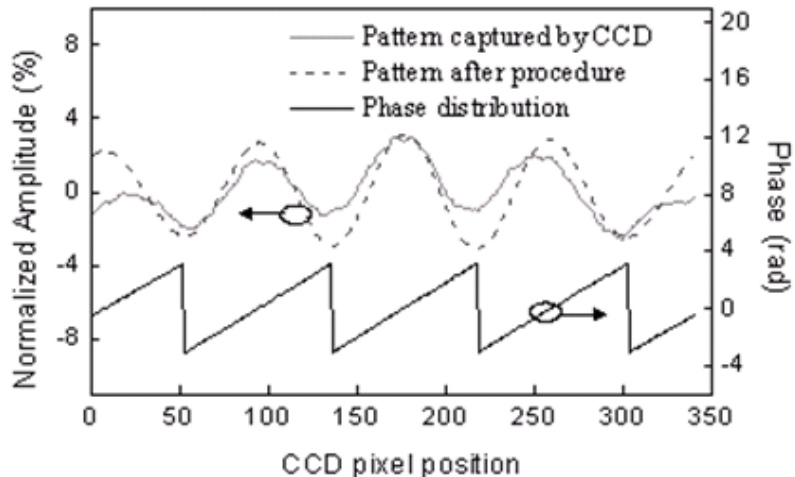


Fig.3.4 Typical 1D interference pattern captured by CCD, the pattern after processing and the calculated phase distribution.

In practice, the whole algorithm is implemented with the LabVIEW software for automatically controlling the whole measuring process. The accurate movement of one period is achieved by shifting the translation stage to an approximate distance and then iteratively fine-tuning the PZT stage to match the phase distribution of the interference pattern on the CCD camera. The iteration process terminates when the phase distribution obtained in this step matches that of last step. The resulted accurate amount of movement is recorded by the Michelson interferometer.

The sample period is approximately 1357 nm from the measurement. The period should keep the same value when the sample is rotated 60 degree due to geometric symmetry. Fig.3.5 indicates reasonable data trend as expected.

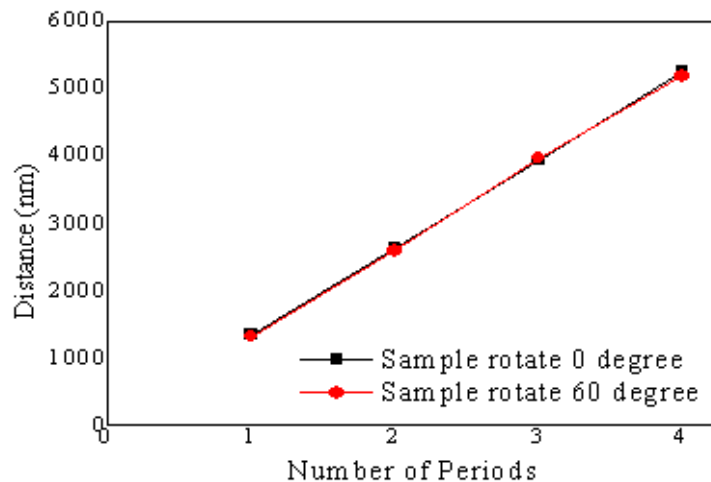


Fig.3.5 Number of period versus translational distance for HPCG crystal axis placed at 0° and 60°.

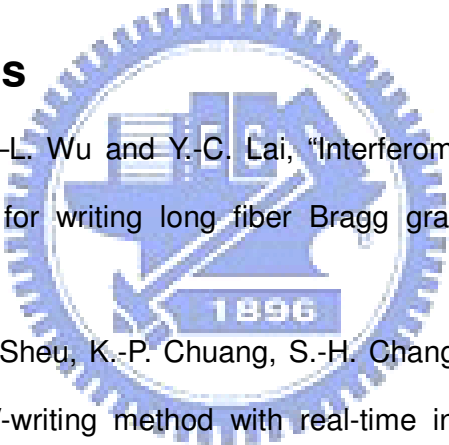
We further investigate the position monitoring accuracy by introducing different phase shifts within one period. Fig.3.6 lists the statistical data for average displacement and standard deviation of total 50 measurements per phase shift. In our preliminary experimental setup, the position monitoring accuracy of the whole system is better than 1.8nm, which means the accuracy of the position-seeking feedback control loop is set to be 0.5 degree of the array period. From Fig.3.6, an 8 nm

movement (2 degree phase shift with respect to one period of the HPCG sample) can be easily detectable with 0.94nm uncertainties.

	Phase shift (degree)				
	2	5	60	180	360
Average displacement (nm)	8.12	19.06	439.67	664.51	1357.51
Standard deviation (nm)	0.94	1.65	5.70	12.63	18.03

Fig.3.6. One-dimensional position monitoring statistics according to the amount of phase shifts with respect to one period

### 3.3 References

- 
- [3-1] K.-P. Chuang, I.-L. Wu and Y.-C. Lai, "Interferometric side-diffraction position monitoring technique for writing long fiber Bragg gratings," CLEO/IQEC, CThM6 (2004).
- [3-2] K.-C. Hsu, L.-G. Sheu, K.-P. Chuang, S.-H. Chang and Y.-C. Lai, "Fiber Bragg grating sequential UV-writing method with real-time interferometric side-diffraction position monitoring," Opt. Express 13, 3795-3801 (2005).
- [3-3] K.-C. Hsu, L.-G. Sheu, and Y.-C. Lai, "Fabrication of Fiber Bragg Gratings by Sequential UV-Writing with Real-Time Interferometric Side-Diffraction Position Monitoring", ECO2005, We4.P.132.
- [3-4] F. El-Diasty, A. Heaney, and T. Erdogan, "Analysis of fiber Bragg gratings by a side-diffraction interference technique," Appl. Opt. 40, 890-896 (2001).
- [3-5] K.-C. Hsu, C.-C. Chen, C.-H. Chan, P.-F. Chung, Y.-C. Lai, "Simultaneous two-dimensional nanometric-scale position monitoring by probing a two-dimensional photonic crystal plate," OPT 2008, Taipei, paper Sat-S8-03.

# Chapter 4

## Experiment of two-dimensional measurement

The aim of this work is to achieve simultaneous two-dimensional nanometric-scale position monitoring in a simple and cost-effective interferometric setup. We will present our experimental results of two-dimensional nanometric position measurement in this Chapter. The first part of this Chapter is the experimental setup, and the second part is the description of the monitoring program, and the final part is the demonstration of the measurements and results.

### 4.1 Experimental setup

#### 4.1-1 Components of the interferometer

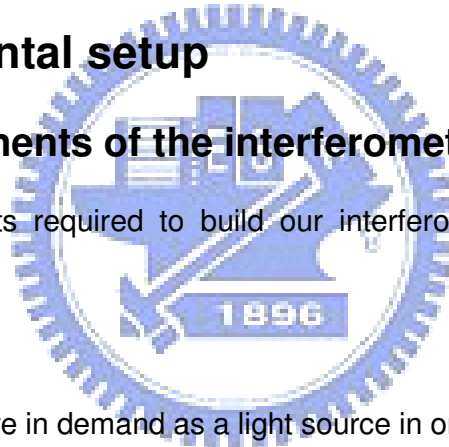
Several components required to build our interferometer system are described below:

##### 1. Light source

In general, lasers are in demand as a light source in order to make interference. For continuous measurements, gas lasers are suitable because of their long coherent length [4-1].

In our experiment, the Helium neon laser is used. The coherent length of a Helium neon lasers with a low power (2-50 m W ,  $\lambda=632.8\text{nm}$ ) is 15-22cm. The coherence length, an important property in interferometry, is the optical path difference between the two interfering beams for which the fringe visibility falls to zero [4-2]. It is an important condition for arranging the optical components of three beams to yield a visible interference fringe.

##### 2. Diffraction grating



In our measurement, the hexagonal photonic crystal glass is regarded as a two-dimensional diffraction grating.

### 3. Beam expander

A beam expander consists of an input objective, a lens and a pinhole shown on Fig.4.1. The pinhole is placed at the focus of the objective. This spatial filter provides a simple way to block out random fluctuations from the intensity profile of the laser beam [4-2]. For the purpose to obtain a suitable beam size, the beam expander is arranged in our system.

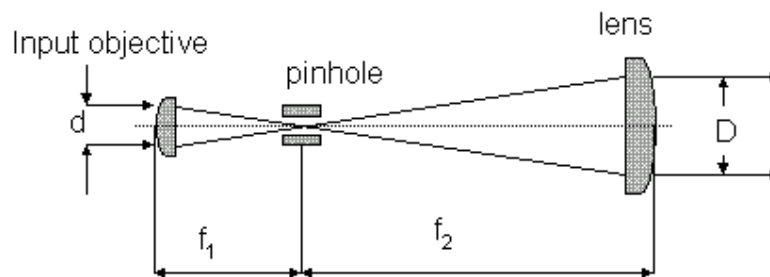


Fig.4.1 Beam expander

### 4. Mirrors, Lenses

Mirrors are required to reflect the diffraction beams to the same plane for interference. In order to avoid light power losses through reflection and absorption and to enhance mechanical stability, generally, as few mirrors as possible should be used [4-1].

### 5. Polarizer

A polarizer is a device that converts an unpolarized or mixed-polarization beam of electromagnetic waves into a beam with a single polarization state. These devices may vary in effectiveness and some of them may be called leaky or partial polarizers [4-3]. In our experiment, polarizers are inserted in order to adjust the intensity of beams.

## 6. Half-wave plate

A wave plate is an optical device that alters the polarization state of a light wave traveling through it. A half-wave plate, a common type of wave plate, retards one polarization by half a wavelength, or 180 degrees. In our experiment, half-wave plates are inserted in order to rotate the polarization.

### 4.1-2 Interferometer for measuring displacement in two-dimension

Fig.4.2 displays the experimental setup and Fig.4.3 shows the actual experimental setup for two-dimensional measurement. To show the feasibility of our system, the displacement provided by two linear stages was measured. The HPCG plate regarded as a diffraction grating is mounted on these two crossed linear stages. The movement accuracy of both stages is 4nm. By controlling stages, HPCG can make translational movement in two-dimension. A single-polarization 633-nm laser beam is focus on the HPCG plate with a spherical lens of 125-mm focal length. For measuring two-dimensional translational movements, we choose three beams, including one zero-order diffraction beam and two first-order diffraction beams, to produce a chessboard-like interference pattern. Therefore, there are three optical paths from HPCG to CCD camera. The actual optical diffraction pattern is shown on Fig.4.4.

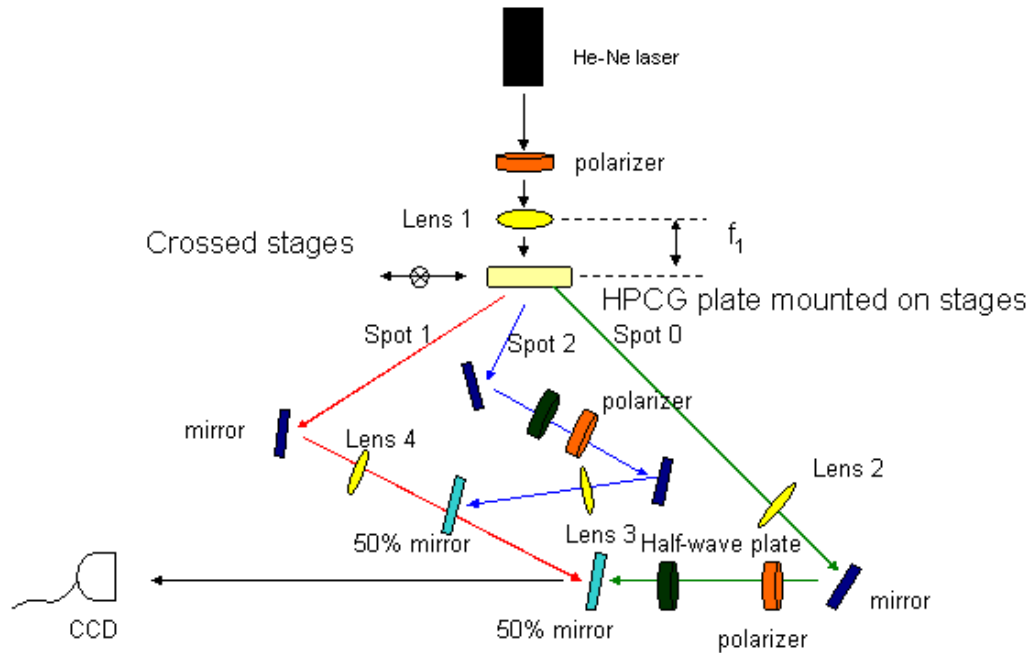


Fig.4.2 Schematic diagram of the experimental setup for two-dimensional measurement

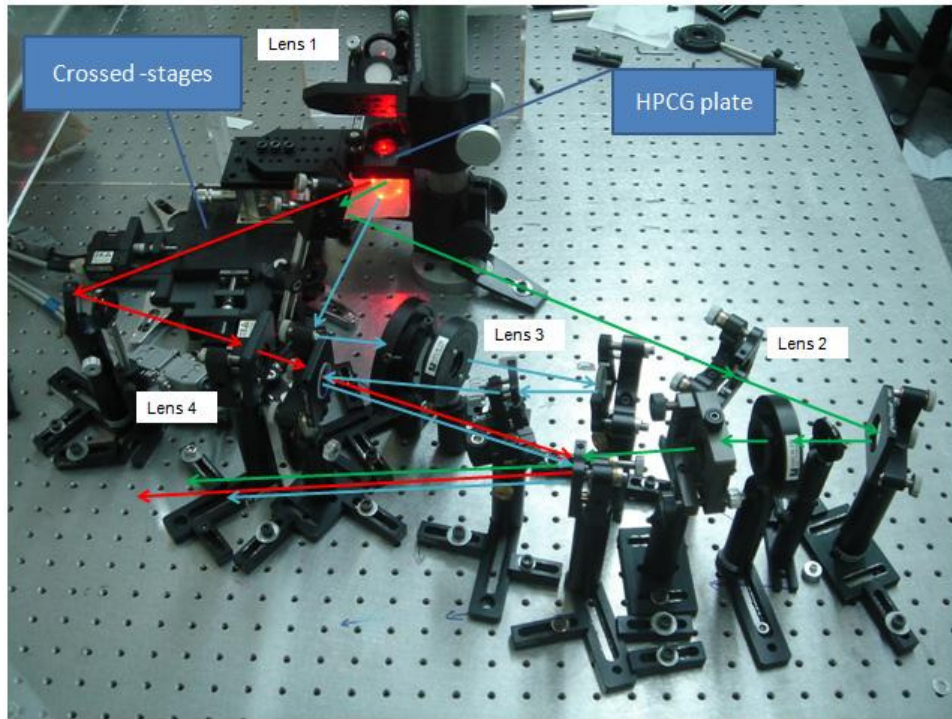


Fig.4.3 The actual experimental setup for two-dimensional measurement



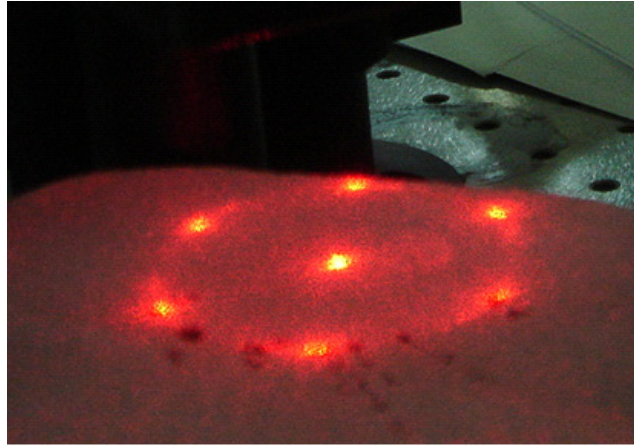


Fig.4.4 The actual optical diffraction image of diffraction pattern in two-dimensional measurement

For getting an interference pattern as clear as possible, some characteristics have to be noticed. First, to obtain good visibility fringes, the amplitudes of the two interfering beams must be nearly equal. However, there is intrinsic difference on intensity between the zero-order diffraction beam and the first-order diffraction beam. For this reason, the polarizer is used to modulate the intensity of beams. Nevertheless, a polarizer not only will decrease the intensity, but also will change the polarization. In order to get effective interference phenomena, the polarization of three beams must be on the same plane. For this purpose, a half-wave plate is placed in order to rotate the polarization. In use of these two optical devices (polarizers and half-wave plates), the analyzable interference is easily obtained.

Thinking about the interference pattern of these three beams to be monitored by a CCD camera, we have to consider about the beam size. The CCD camera we used is a 640×480 monochrome CCD camera with a pixel width of 9.2- $\mu\text{m}$ . When the size of the beam is 3mm, pixels of CCD can be effectively used, and all these data can be effectively analyzed. The beam size of the 633nm He-Ne laser beam is approximately 1 mm, and the beam width after focusing onto the HPCG sample is calculated to be

24 $\mu$ m. To obtain a 3mm beam size, it is necessary to expand the beam. In Fig4.2, the focal length of the first lens (lens 1) is 125-mm, and the focal length of the others ( lens 2,3,4) is 400- mm. In this arrangement, the size of the beam can be expanded to approximately be triple, 3.2 mm, right suitable for us to monitor the interference pattern.

Because one of the key factors for displacement resolutions of the whole system is determined by the resolution of the CCD camera, the larger fringe period produces the improved displacement resolution. The interference angle of two beams, which producing interference, must be very small in order to get large fringe period on the CCD camera. We simply use 50% mirrors to combine them. The zero-order beam and one of the first-order beams can propagate in nearly the same optical path between the 50% mirror and the CCD camera by carefully aligning.

Adjusting the incidence angle on the CCD camera can change the distribution of the interference pattern. For the ease to observe, we modulate respectively a horizontal periodic interference pattern and a perpendicular periodic interference pattern shown on Fig.4.5 (b) and (c). These two interference patterns are formed by interfering the zero-order beam with the first-order beam. Then, the net pattern becomes a chessboard-like pattern shown on Fig.4.5 (a). The optical phase variation resulting from the movement of grating can be measured by this optical interferometer. Besides, there is another undesired oblique periodic interference pattern formed by the two first-order beams as shown on Fig.4.5 (d).

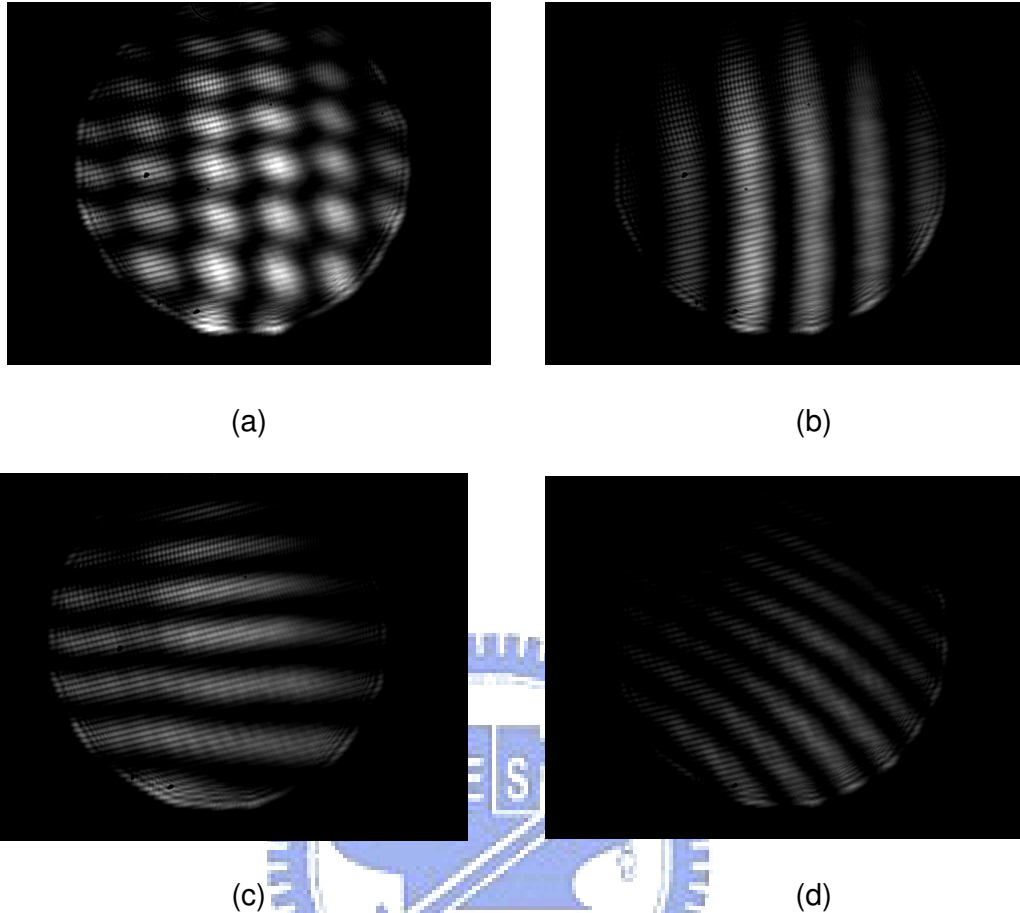


Fig.4.5 The actual interference pattern caught by the CCD camera (a) the measured chessboard-like interference pattern(b)formed by the zero-order beam and the first-order beam(c) formed by the zero-order beam and the first-order beam(d) formed by two first-order beams

## 4.2 Monitoring program

To analyze the interference pattern, the system is implemented with the LabVIEW software for obtaining the phase information. First, we transform the picture captured by the CCD camera to an array, shown on Fig.4.5, which we can analyze by the LabVIEW software.

FFT is a general method proposed for the analysis of the fringe pattern. The flow

chart of the FFT algorithm is shown in Fig.4.6 [4-5]-[4-6]. First, the interference pattern is processed by the FFT to obtain the corresponding spatial frequency spectrum. After FFT, we need to separate the picture array to four parts from the origin and rearrange these four parts to get the pattern with a peak in the central area shown on Fig4.7. This arrangement is for avoiding the problem of fast variation term.

From Fig.4.7, we can find one peak (the highest one) at the origin presenting the DC term. It indicates the average background. The others surrounding the origin present the AC terms. And, in the  $\xi$ -axis direction, the peak beside the central (peak 2) comes from the periodic function in the x-axis direction as mentioned in 2.3-1. Similarly, in the  $\eta$ -axis direction, the peak beside the central (peak 3) comes from the periodic function in the y-axis direction. The separation between peak 1 and peak 2 or peak 3 depends on the period of interference pattern in the x- or y- directions. These peaks bring the phase information of interference pattern. When the HPCG moves, the phases of the zero-order beam do not change. However, the phases of the first-order beams will change. Therefore, we can find displacements of the HPCG from the phase difference between the zero-order and the first-order components before and after the HPCG moving. The required phases can be calculated from the peak points in the complex spatial-frequency spectrum.

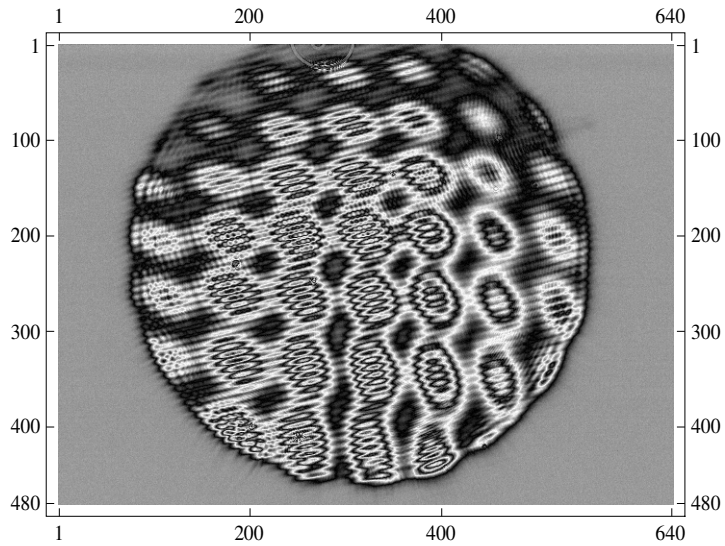


Fig. 4.5 The image transformed from the measured chessboard-like interference pattern by the LabVIEW software.

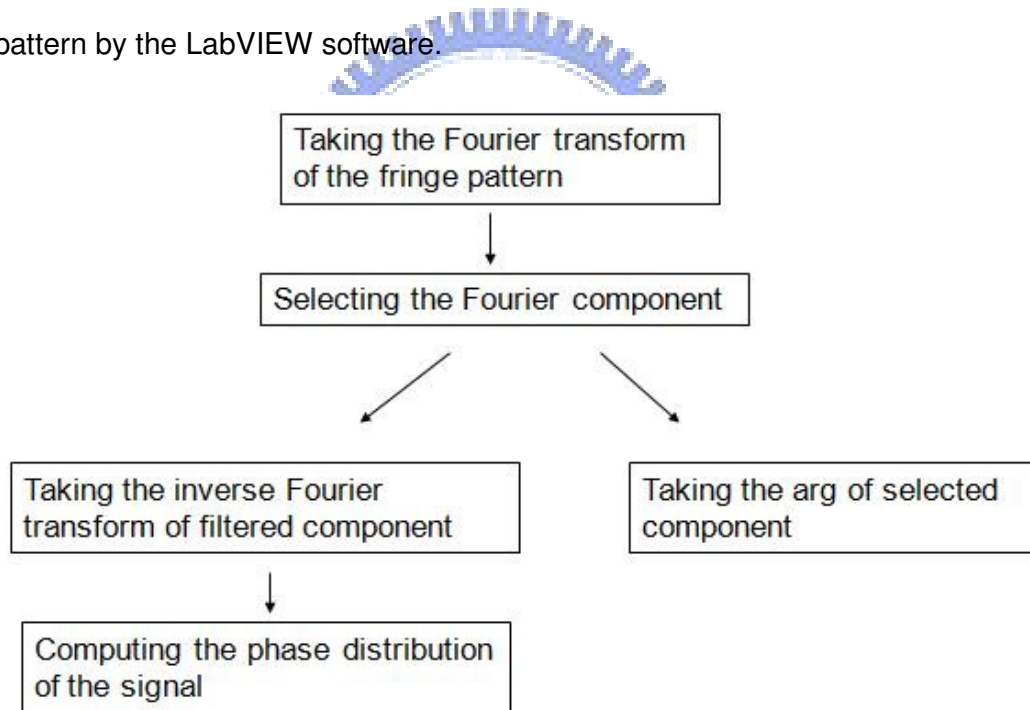


Fig.4.6 The flow chart for FFT algorithm

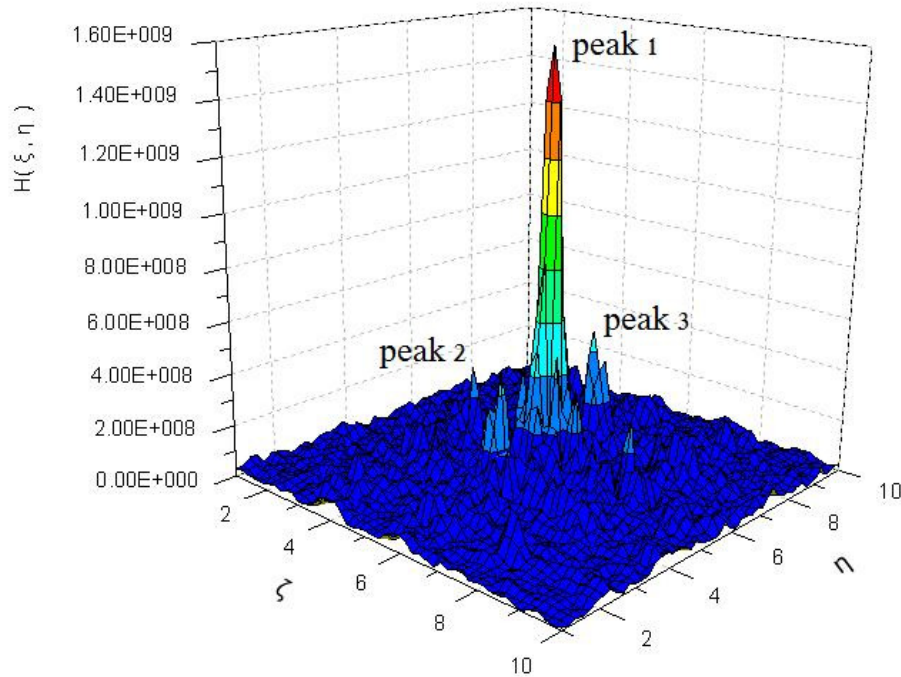


Fig.4.7 The complex spatial-frequency spectrum of the interference pattern

For obtaining the phase changes from the complex spatial-frequency spectrum, filtering techniques can be used. The spectrum is then filtered to keep only the positive frequency part. We choose two points from the Fourier spectrum, including the point at origin (peak 1) and the point beside the origin one with the highest peak (peak 2 or peak 3), to be processed by the inverse Fourier transform to back to the original domain. Then, we can obtain a distinguished 1D interference pattern shown on Fig4.8. It is the result after filtering out all the undesired noises and signals. From this pattern, we can monitor the real-time phase changes. The point we choose from the  $\xi$ -axis direction and the  $\eta$ -axis direction can respectively produce the x- and y-direction interference patterns. Comparing the difference of the filtered interference fringes before and after moving, the phase changes can be decided. Besides, from the filtered interference pattern, the measurement resolution is approximately 20nm.

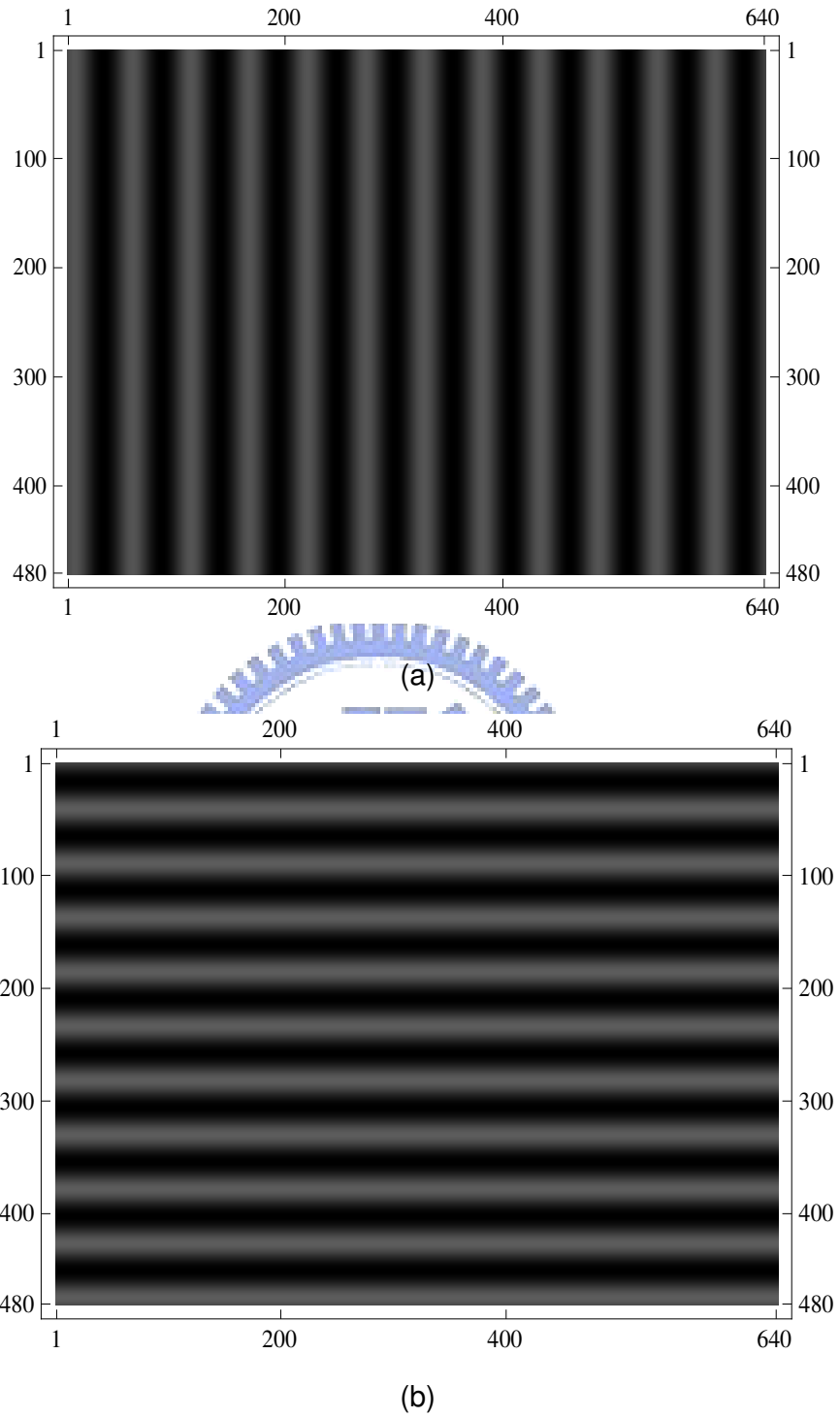
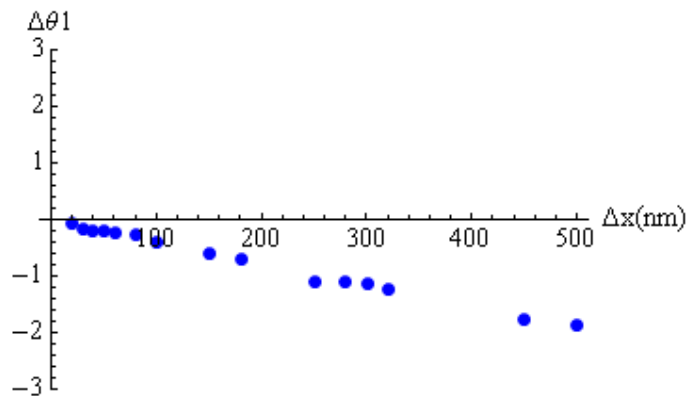


Fig.4.8 The filtered interference pattern (a) in the x-direction (b) in the y-direction.

## 4.3 Measurements and results

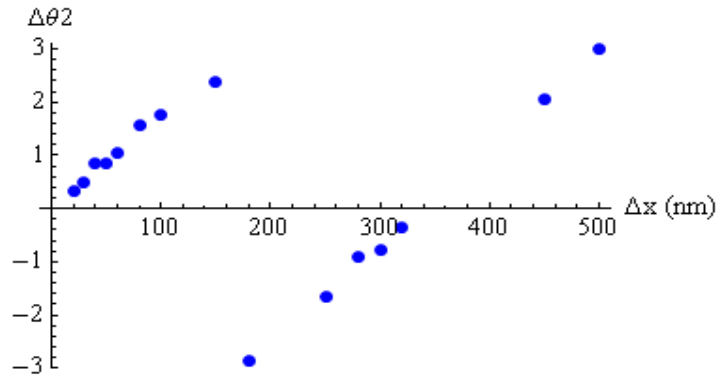
### 4.3-1 Determining the transform matrix

To find the relation between the phase changes and displacements, we preliminarily move one stage to make the diffraction grating experience one-dimensional movement. We record the phases before and after moving the stages. To avoid confusion, we restrict all the phase to be between  $\pi$  and  $-\pi$ . The plots of the phase changes  $\Delta\theta_1$  and  $\Delta\theta_2$  as a function of  $\Delta x$  with  $\Delta y=0$  is shown in Fig.4.9 (a, b). Fig.4.9 (c, d) show the plots of the phase changes  $\Delta\theta_1$  and  $\Delta\theta_2$  as a function of  $\Delta y$  with  $\Delta x=0$ . As is shown in Fig.4.9, the phase changes are linearly periodic with respect to the position displacement. We thus confirm that the variation of the phase changes is as expected when performing different movements. Besides, it should be noticed that it is necessary to plus or subtract  $2n\pi$  when the displacement exceeds one period. After this process, one obtains Fig.4.10. From Fig.4.10, one displacement value will be corresponding to one phase change value.

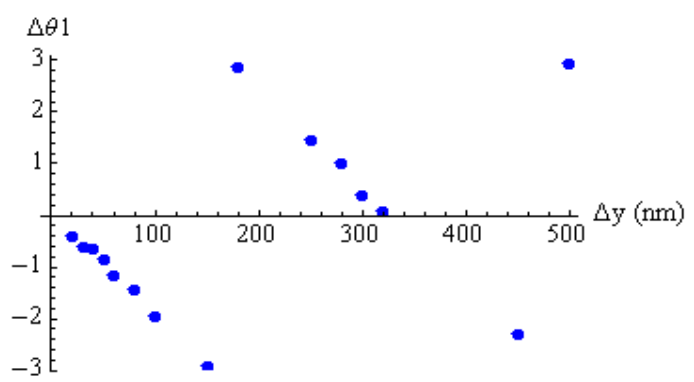


(a)

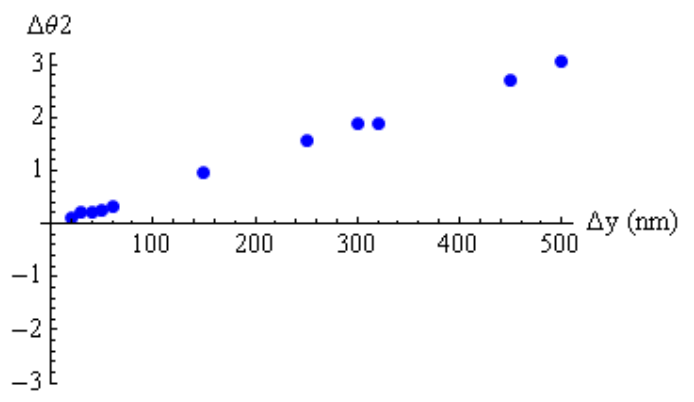




(b)

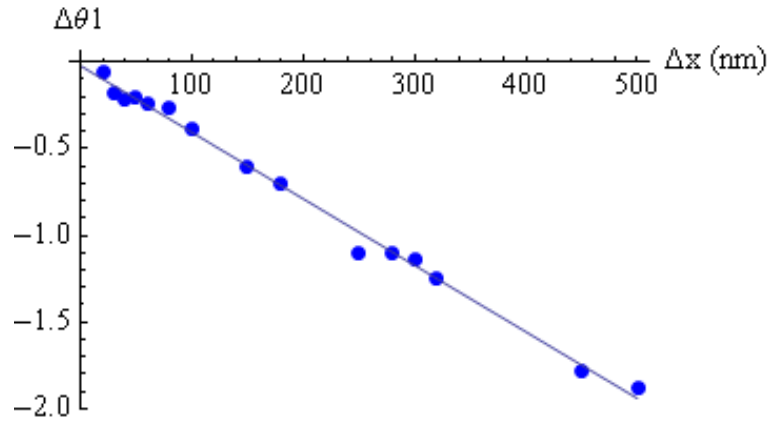


(c)

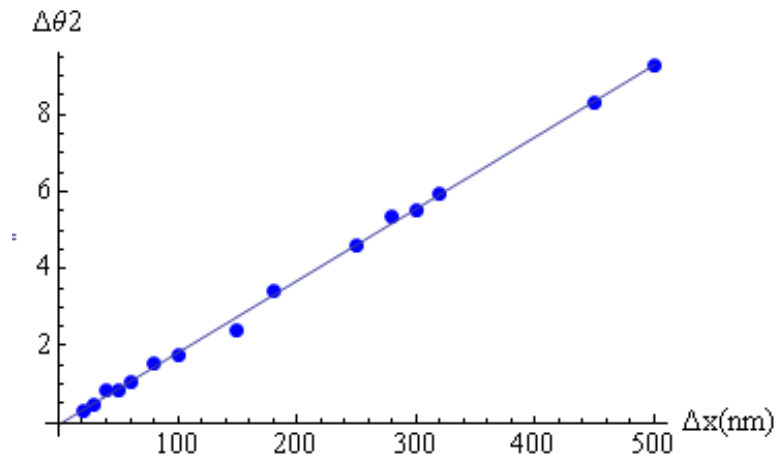


(d)

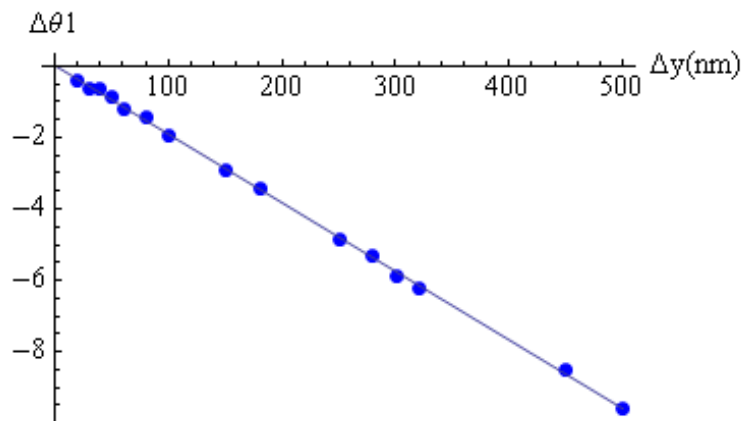
Fig.4.9 The original plot of phase-changes versus displacement (a) Variation of x displacement with x phase change(b) Variation of x displacement with y phase change(c) Variation of y displacement with x phase change(d) Variation of y displacement with y phase change



(a)



(b)



(c)

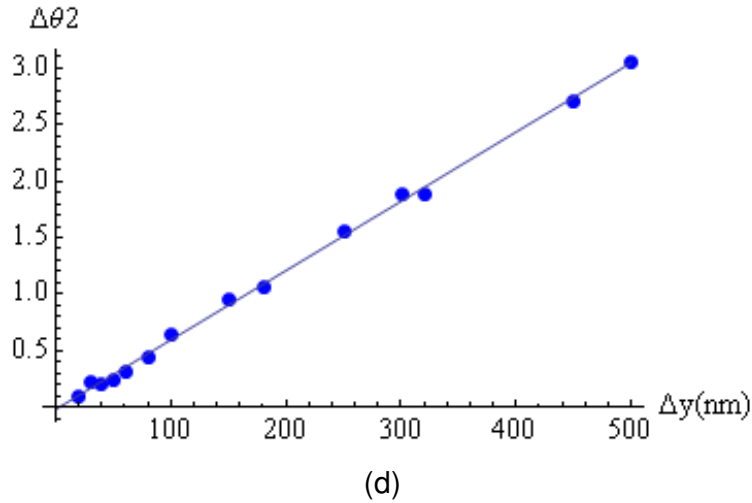


Fig.4.10 The chart of phase-changes versus displacement after correcting the phase-change value(a) Variation of x displacement with x phase change(b) Variation of x displacement with y phase change(c) Variation of y displacement with x phase change(d) Variation of y displacement with y phase change

From Eq.2.19, the data of  $(\Delta x, \Delta y, \Delta\theta_1)$  can contribute to a plane. From the fitted plane of those data, we can find the elements  $M_{11}$  and  $M_{12}$  of the transform matrix. Similarly, the elements  $M_{21}$  and  $M_{22}$  can be obtained from the plane equation of  $(\Delta x, \Delta y, \Delta\theta_2)$ . Then, we find the whole transform matrix shown in Eq.4.2. For the ease to figure out displacements from phase- changes, the matrix is processed by the inverse transform to obtain the final formula between displacements and phase-changes as follows :

$$\begin{aligned} \begin{bmatrix} \Delta x \\ \Delta y \end{bmatrix} &= \begin{bmatrix} M_{11} & M_{12} \\ M_{21} & M_{22} \end{bmatrix}^{-1} \begin{bmatrix} \Delta\theta_1 \\ \Delta\theta_2 \end{bmatrix} \\ &= \begin{bmatrix} 71.26 & 227.81 \\ -221.67 & -47.47 \end{bmatrix} \begin{bmatrix} \Delta\theta_1 \\ \Delta\theta_2 \end{bmatrix} \end{aligned} \quad (4.1)$$

### 4.3-2 Measurement of two-dimensional movement

To test the accuracy of the transform matrix that we figure out from one-dimensional measurements described on 4.3-1, several sets of two-dimensional measurements are performed. The average phase-changes for different two-dimensional movements are substituted into Eq.4.2 to obtain the measured displacements. The statistics presented in Fig.4.11 shows that the difference between movements of stages (red points) and measured results (black points). Detailed data, including standard deviation, are listed in Fig.4.12. From Fig.4.12, we can find that the accuracy deteriorates with increasing measured length. The standard deviation shown in Fig.4.12 grows, when the distance of movement increases. The results also imply the best accuracy of our system for simultaneously two-dimensional movement is approximately 20nm.

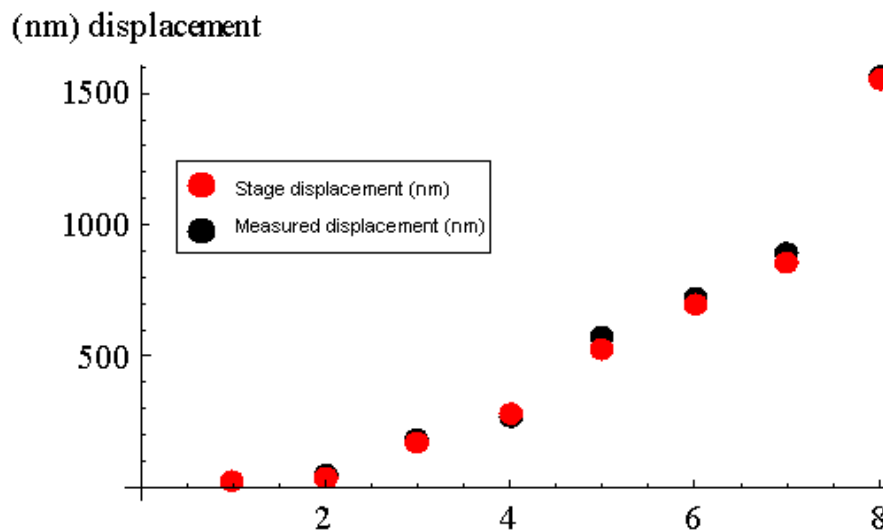


Fig.4.11 The results of two-dimensional measurements by probing the HPCG plate. Red one presents stage displacements, and black one presents measured displacements.

Grating Displacement (nm)	Measured Displacement (nm)	Standard Deviation (nm)
28	19	19
44	35	19
178	173	27
268	285	37
576	527	47
721	699	80
894	850	81
1562	1554	82

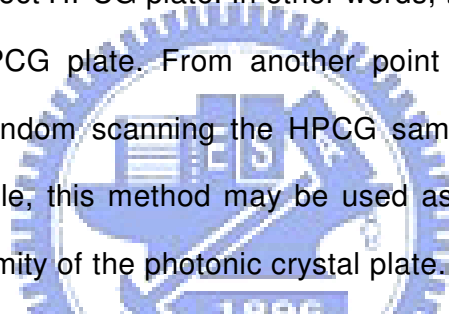
Fig.4.12 Statistics for sets of two-dimensional movements

### 4.3-3 Analysis

In the measurement, when the HPCG sample moves, the laser beam will scan an area of the HPCG plate instead of the same position. Suppose that our system has the potential to perform two-dimensional long-distance displacement measurement, the laser beam will be incident on very different points of the HPCG plate for each measurement. The laser beam would scan the HPCG randomly and might scan over the whole plate. However, it is possible that some uncertainties come from the distortion in the periodic structure of the HPCG plate. From the SEM picture of the HPCG shown in Fig.3.1 (a), we can find that the structure is not so perfectly periodic in the used sample. Therefore, the following measuring method is designed to observe the influence by the uniformity of the HPCG plate.

To confine the probing area to a small part, we control the stages to move a round trip. In this way, the influence of the HPCG plate would be reduced. Then, the following measurement procedures are performed in the same way mentioned before. Fig.4.13 shows the results of scanning certain area and also lists the

results of scanning the HPCG plate randomly. From Fig.4.12, a 1562nm movement is measured to 1614nm with 20.435nm uncertainties by the method of probing in the same position, and 1554nm with 82.71nm uncertainties by the method of scanning diffraction grating randomly. The comparison indicates that confining the probing region could be advantageous to obtain more accurate measurement results and the standard deviation is not increasing with the increasing distance of movement. Therefore, the results support that the accuracy is improved by the way of remaining the incident laser beam in a tiny part of the diffraction grating. We conclude that the measured results will depend on where the laser beam probes into due to the imperfect HPCG plate. In other words, the accuracy depends on the uniformity of the HPCG plate. From another point of view, since the position reading errors for random scanning the HPCG sample is due to the uniformity problem of the sample, this method may be used as a simple optical means for monitoring the uniformity of the photonic crystal plate.



Displacement (nm)	Scan randomly		Scan certain area	
	measuring result (nm)	Standard deviation (nm)	measuring result (nm)	Standard deviation (nm)
178	173	27	173	14
288	285	37	276	17
1562	1554	82	1614	20

Fig.4.13 Comparison between two different methods (a) scanning the HPCG plate randomly, (b) scanning it into certain small area.

For confirming the influence by the uniformity of the diffraction grating, we replace the HPCG plate with a blazed grating (BG) provided by the ITRI group, which is more uniform but the period is bigger, 83.5 $\mu$ m. To make the BG on a PET film, a mechanically grooved structure was first formed on a printing roller, which was made

by using a roller cutter with the designed profile, as shown in Fig. 4.14(a). Then the UV resin was dispensed on the PET film, imprinted by the roll, and cured with UV source, as shown in Fig. 4.14(b) [4-4]. The diffraction pattern of BG is shown in Fig. 4.15. The clear diffraction pattern can be obtained without the beam focusing into the blazed grating. Remind that in the setup of probing the HPCG plate, the beam has to be focused into the HPCG plate, otherwise a visible pattern can't be formed, This should be caused by the less periodicity of the HPCG. When the beam is focused, the size of beam becomes smaller. Therefore, the area of being probed is smaller, and thus comparatively more periodic to yield clear diffraction patterns.

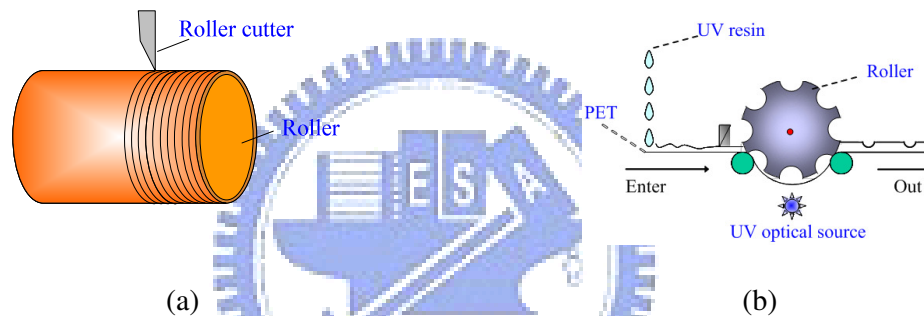


Fig. 4.14 To make the BCSG on a PET film, a mechanically grooved structure was first formed on a printing roller using a roller cutter with the designed profile as shown in (a). Then the UV resin was dispensed on the PET film, imprinted by the roll, and cured with UV source as shown in (b).

The diffraction pattern from probing the blazed grating is shown on Fig.4.15. Repeating the same measurement procedure mentioned above, the statistics are listed in Fig.4.16. The standard deviation didn't increase with the distance of movement now. For the reason that there is a better periodic surface for the blazed grating, this is an expected result. We conclude that better uniformity of the diffraction grating can improve the uncertainties of measurements. However, as one can see by comparing Fig. 4.12 to Fig. 4.16, the large period of the blazed grating limits the scale of the measurable displacement and resolution. Thus, the

smaller period of the probing sample is required for performing delicate position monitoring.

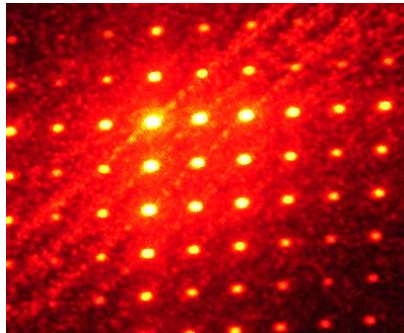


Fig.4.15 The diffraction pattern of probing the blazed grating

Grating displacement(nm)	Measured displacement(nm)	Standard deviation (nm)
1000	1710	1313
4000	4181	2404
6000	6110	2269
8000	8070	2867
10000	11280	2405
14000	13515	2639
16000	17004	2863
20000	19554	2811
26000	25560	2273
28000	28190	2445
30000	30666	1978

Fig.4.16 The statistics of measurement by probing a blazed diffraction grating, the period of which is 85 $\mu$ m

### 4.3-4 Discussion

To observe the stability of our system, we record the phase values without moving the diffraction grating. As is shown in Fig.4.17, the phase is not stable. As we know, the optical interferometer used in non-isolation always suffers from large errors or noise, most from atmospheric influences, background vibration, and



thermal drift.

The final data we need is the comparison before and after moving the stages. Therefore, we perform measurements in a very short time period to keep the environmental condition being the same. For long term running, decreasing the environmental fluctuations will be the most important requirement of the current experiment.

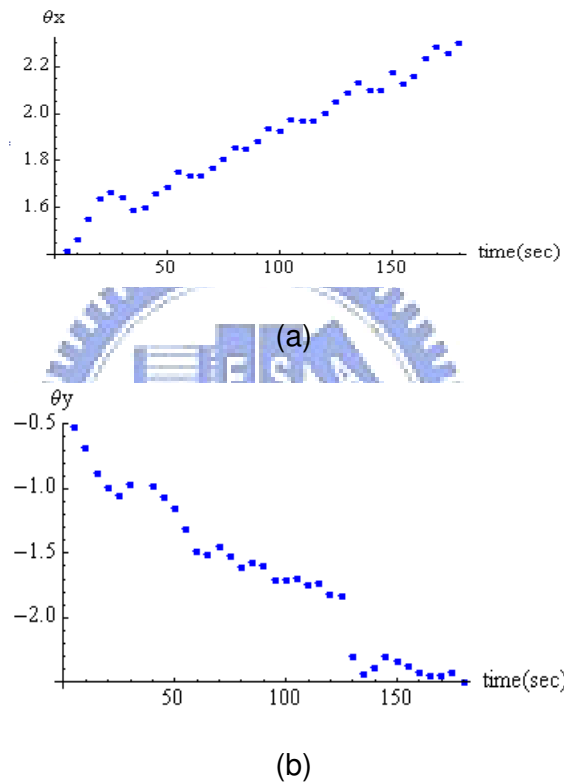


Fig.4.17 The disturbance of phase caused by environment (a) in the x-direction (b) in the y-direction

Except for the disturbance of environment, the minimum detectable translation movement and the position accuracy of the whole system are mainly limited by the wavelength of the probe laser beam and the period of the photonic crystal plate. In principle, it can be down to nanometric-scale for long range position monitoring under the condition that the sample can be highly uniform over large scale.

In the view of signal processing, if we could obtain an interference pattern from the

higher order beams, the signal of the phase information would increase. In this way, the measurement resolution can be better and the minimum detectable measurement can be smaller. However, the intensity of the higher-order diffraction beams of the HPCG may not be strong enough to yield an interference pattern. In conclusion, except for improving the set-up of interferometer, the improvement of diffraction grating also can be very advantageous for the measurement system.

## 4.4 References

- [4-1] F. Mayinger (Ed.), "Optical measurements : techniques and applications", Berlin Springer-Verlag press 1994.
- [4-2] P.K. Rastogi, (Ed.), "Optical measurement techniques and applications", Boston Artech House press 1997.
- [4-3] E. Hecht, "Optics", fourth edition, San Francisco Addison Wesley press 2002.
- [4-4] H.-H. Lin, C.-H. Lee, M.-H. Lu, "Dye-less color filter fabricated by roll-to-roll imprinting for liquid crystal display applications", OSA (2009)
- [4-5] M. Wang, "Fourier transform method for self-mixing interference signal analysis", Opt. Laser Technol. 33 (6) 409 (2001).
- [4-6] M. Takeda, H. Ina, S. Kobayashi, "Fourier-transform method of fringe-pattern analysis for computer-based topography and interferometry", Opt. Soc. Am. 72, 156-160 (1982)

# Chapter 5

## Conclusions and future work

### 5.1 Conclusions

In this thesis, real-time interferometric two-dimensional nanometric-scale position monitoring is proposed and demonstrated via a simple two-dimensional interferometric setup by probing a two-dimensional hexagonal photonic crystal plate. To real-time monitor the two-dimensional translational movement in the nanometric-scale, an optical imaging system is built by probing a hexagonal photonic crystal glass (HPCG) with a 633-nm He-Ne laser beam. The translation movements in both directions are recorded in the phases of the fields of the diffracted six spots. By carefully aligning the first-order two spots and the zero-order spot to form a chessboard-like interference pattern on the CCD camera, the individual nanometric-scale movement information can be determined by the phase-changes of the chessboard-like interference pattern before and after moving. In principle it can attain the nanometric-scale accuracy of position reading in both orthogonal moving directions. Thus the simultaneous two-dimensional nanometric-scale position monitoring is achieved in a simple and cost-effective interferometric setup, and the minimum detectable translational movement is dependent on the period of the probed photonic crystal, and can at least be down to 20nm as demonstrated in the present work.

### 5.2 Future work

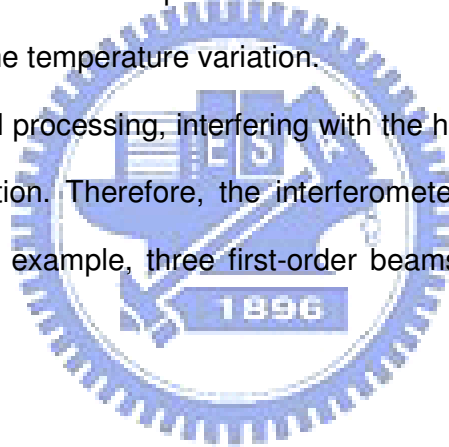
To attain a two-dimensional nanometric-scale position monitoring system with high performance, there may be three key factors for the future improvement of the present

proposed measurement system. They are the uniformity of the gratings, the reduction of environmental noises and the use of high order diffraction beams.

The uncertainties of the measurement depend on the uniformity of the diffraction grating directly. Therefore, the better uniformity of the diffraction grating period, the longer displacement we can measure. To apply our system for longer distance measurement, we should use grating samples with as small and uniform period as possible.

Besides, as mentioned in 4.3-4, the unstable temperature, which would cause the optical table or components to expand or shrink, disturbs our measurements. Therefore, in principle with a temperature monitor one could compensate the error signal resulted from the temperature variation.

In the view of signal processing, interfering with the higher order beams can obtain better phase information. Therefore, the interferometer with the selection of other diffraction beams (for example, three first-order beams) can be approached in the future.



#### Acknowledgement

The author gratefully thanks Prof. Chii-Chang Chen at the Department of Optics and Photonics, National Central University for providing the HPCG plates, and Dr. Chi-hung Lee at the Mechanical and Systems Research Laboratories, Industrial Technology Research Institute, for providing the blazed grating samples.